J Solid State Electrochem (2012) 16:3401–3421
DOI 10.1007/s10008-012-1876-3

REVIEW

Oxygen solid electrolyte coulometry (OSEC)

V. Vashook · J. Zosel · U. Guth

Received: 29 March 2012 / Revised: 6 July 2012 / Accepted: 16 July 2012 / Published online: 5 October 2012

Abstract The development and utilization of solid electrolyte-based coulometric techniques for the investigation of different oxygen exchange processes of solids or liquids, oxygen or hydrogen permeability through membranes, and generation of gas flows with well-defined oxygen concentration is briefly reviewed. The method based on Faraday's law may be used alternatively or additionally to thermogravimetry, gas chromatography, chemical analysis, spectroscopy, and X-ray or neutron diffractometry in a wide oxygen partial pressure region (10^{-20} to 10^{5} Pa) unaffected by temperature. The detection limit of exchanged oxygen is determined by a current- and voltage-measuring technique and is now not lower than 50 ng for devices operating in carrier gas mode.

Keywords Oxygen solid electrolyte coulometry · Oxygen nonstoichiometry · Oxygen permeability · Oxygen concentration

Introduction

Coulometry is a group of techniques in analytical electrochemistry for the quantitative determination of substances by means of electrolysis reactions. It is based on counting the electrons and subsequently the mass transported through the electrochemical cell by an electrochemical reaction. At first, this method was developed for liquid systems [1, 2]. Inorganic and organic substances can be analyzed if any corresponding reaction can be conducted in an electrochemical cell.

This technique is based on electrolysis, and it attempts to completely oxidize or reduce the whole electroactive analyte species to a new known state in a volume of sample solution.

V. Vashook · J. Zosel · U. Guth (✉)
Dresden University of Technology,
Dresden, Germany
e-mail: guth@ksi-meinsberg.de

Due to the quantitative relationship between electrical charge and the mass transported (Faraday's law), the method requires no calibration. Electrolysis can be conducted at constant current or at constant voltage.

The electrical charge Q measured in coulombs of electricity transferred during the electrolysis process can be determined generally as:

$$Q = \int_{t_1}^{t_2} I(t) \cdot dt \tag{1}$$

where $I(t)$ is the current and t is the electrolysis time.

If only one reaction occurs in the electrochemical cell, this electricity can be related to the converted amount (m) of substances in grams according to Faraday's law as follows [3]:

$$m = \frac{M}{z} \cdot \frac{Q}{F} = \frac{M}{z} \cdot \frac{\int_{t_1}^{t_2} I(t) \cdot dt}{F} = N \cdot \frac{\int_{t_1}^{t_2} I(t) \cdot dt}{F} \tag{2}$$

where M is the molar mass, z is the number of electrons transferred per molecule of analyte, F is the Faraday's constant (96,487 C mol^{-1}), and N is the electrochemical equivalent of analyte in grams per mole of transferred electrons.

This analytical method is known as coulometry. During coulometry at constant potential, the total amount of charge (Q) is obtained by integration of the current $I(t)$ curve as a function of t or Q can be determined directly by using a coulometer (electronic integrator).

Solid electrolyte coulometry (SEC) considers the electrolysis reactions in cells using solid electrolytes. In oxygen solid electrolyte coulometry (OSEC), solid oxide electrolytes such as yttria-stabilized zirconia (YSZ), cerium oxide (CeO_2), perovskite-based conductors ($La_{0.8}Sr_{0.2}Ga_{0.8}Mg_{0.2}O_{3-\delta}$), or others are used (Fig. 1). This article focuses only on gas coulometry using solid electrolyte as a quantitative method for the precise and easy determination of oxygen exchanged between gas and solid (or liquid) phases in different processes.

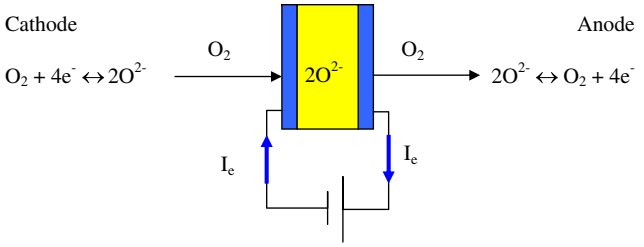

Fig. 1 Schematic presentation of the OSEC method

Oxygen transport in the form of O^{2-} ions through gas-tight oxide solid electrolyte membranes in these cells occurs with the equivalent transport of electrons in the extrinsic circuit only if the electronic conductivity of the solid electrolyte can be considered for most cases as negligible. The temperature of such electrochemical cells should be sufficiently high for the efficient transport of oxide ions and kinetics of the electrode reactions.

The electrode reactions in the electrolysis process shown in Fig. 1 are in reality much more complex because they contain many distinct steps, such as adsorption–desorption, decomposition–formation of oxygen molecules, diffusion of oxygen atoms to the three-phase boundaries, ionization–deionization of oxygen atoms (ions), and incorporation–reincorporation of oxygen ions (O^{2-}) into and out of the bulk solid electrolyte. In electrolysis, the precise mechanism of oxygen exchange and transfer is not important and is, therefore, not considered here.

The mass of oxygen transported through a gas-tight solid electrolyte membrane (m_{O_2}) at 100 % current efficiency can be exactly determined by modifying Eq. 2:

$$m_{O_2} = \frac{32}{96,500 \times 4} \cdot \int_{t=start}^{t=end} I_t \cdot dt \tag{3}$$

where I_t is the current in the cell at the time t. OSEC can be successfully used for:

- Generation of gaseous atmospheres with defined oxygen partial pressure from 10^{-20} to 10^{6} Pa (10^{-25} to 10 atm);
- Quantitative measurements of oxygen exchange between solid and gas or liquid substances in scientific investigations, in the chemical and biochemical industries, in metallurgy, in semiconductor and ceramics production, and with thermogravimetry, chemical analysis, spectroscopy, and X-ray or neutron diffractometry;
- Measurements of oxygen permeability (diffusivity) in ceramic, metal, or polymer membranes;
- Measurement of chemical oxygen diffusion coefficients;
- Determination of humidity of gases;
- Determination of small amounts of hydrogen or hydrocarbons in gas mixtures.

As an alternative to other analytical methods such as spectroscopy and X-ray or neutron diffractometry, SEC does not need calibration for the determination of oxygen content. The oxygen concentration may be easily measured under in situ conditions. Compared with thermogravimetry, SEC allows the determination of actual oxygen exchange in materials even if their thermal treatment is accompanied by mass changes of other species, such as gas or water desorption, fugacity effects, or decomposition. Oxygen exchange measurements can be conducted in quasi-closed systems as well as in open systems.

Oxygen solid electrolyte coulometry in quasi-closed systems

OSEC in quasi-closed systems (Fig. 2) first considers the complete isolation of the material in a minimal chamber with a gas-impermeable solid electrolyte wall attached outside and inside to electrochemically active electrodes. Thus, oxygen can only be quantitatively admitted to the chamber or removed from it by coulometric titration. The chamber may consist completely or partially of solid electrolyte material. Current or assay electrodes (I_{el}) and applied potential electrodes (U_{el}) are insulated from each other using gas-tight high-temperature glass (HTG) seals. The titration current and voltage are simultaneously measurable.

The exchange of oxygen between the solid sample S and the gaseous environment may be determined as a function of temperature and oxygen partial pressure in the known chamber volume. For example, if any solid oxide sample AO_x is placed and sealed at room temperature into an evacuated solid electrolyte cell (Fig. 1), the following reaction should be observed after the cell was heated to a sufficiently high temperature:

$$AO_x \rightarrow AO_{x-\delta} + \delta/2\, O_2 \tag{4}$$

If any equilibrium oxygen partial pressure (pO_2') in the chamber at temperature (T) and oxygen titration current (I=0) is reached, the oxygen content ($x-\delta_1$) of the oxide may be calculated using potentiometry as follows:

$$\begin{aligned} x - \delta_1 &= x - \frac{V \cdot T_0 \cdot M}{11.2 \cdot T \cdot m} \cdot pO_2' \\ &= x - \frac{V \cdot T_0 \cdot M}{11.2 \cdot T \cdot m} \cdot \exp\left(-\frac{4FU_1}{RT}\right) \end{aligned} \tag{5}$$

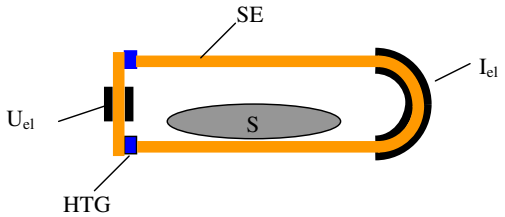

Fig. 2 Schematic representation of the cells for coulometric experiments: *SE* solid electrolyte tube, U_{el} potential electrodes, I_{el} current electrodes, *S* sample, *HTG* high-temperature glass

where V is the volume of the chamber, T_0 is the temperature at standard conditions, M is the molar mass of the AO_x oxide, m is the mass of the sample, pO'_2 is the oxygen partial pressure, U_1 is the voltage in the cell, F is the Faraday's constant, and R is the gas constant. By coulometric titration of oxygen at constant temperature inside or outside the chamber using the current electrodes, the new oxygen partial pressure in the chamber may be established and determined by the potential difference (U_2) measured on the potential electrodes (U_{el}). The change in oxygen content of the solid oxide material ($\Delta\delta_s$) then may be calculated at constant temperature as follows:

$$\Delta\delta_s = \Delta\delta - \Delta\delta_g = \frac{\int_{t=start}^{t=end} I_t \cdot dt}{z \cdot F} - \frac{V}{RT} \cdot \Delta pO_2$$

$$= \frac{\int_{t=start}^{t=end} I_t \cdot dt}{z \cdot F} - \frac{V}{RT} \cdot \exp\left(\frac{-4F \cdot \Delta U}{RT}\right) \quad (6)$$

where $\Delta\delta$ is the total change of oxygen content in the chamber, $\Delta\delta_g$ is the change in oxygen content of the gas phase at the new oxygen partial pressure pO''_2, and ΔpO_2 is the changed oxygen partial pressure in the chamber corresponding to the change in voltage at the potential electrodes U_{el} ($\Delta U = U_2 - U_1$).

The p–T–x diagrams may be constructed for some simple and mixed oxides using this coulometry method. Closed systems allow correct investigations of oxygen nonstoichiometry if all construction elements in the cell are stable and gas-tight. Sealing by HTGs is normally the restrictive element in such cells. Utilization of these systems is typically possible at temperatures 600–800 °C because of the low oxygen conductivity of solid electrolytes below 600 °C and the high oxygen permeation and reactivity of glasses above 800 °C. The range of possible oxygen partial pressures is also restricted by oxygen pressures over 10 Pa.

One of the first attempts to use this technique was described by Tretyakov and Rapp [4] for the determination of nonstoichiometry ranges of $NiO_{1+\gamma}$ and $LiFe_5O_{8-\delta}$. It was shown that the principal defects in $NiO_{1+\gamma}$ are the negative double-ionized nickel vacancies and positive lithium and iron interstitial cations in $LiFe_5O_{8-\delta}$. The γ and δ values as functions of temperature and oxygen partial pressure were determined, and partial molar enthalpies of oxygen in these compounds were calculated and interpreted in terms of the enthalpy of defect formation in these crystals.

A similar solid electrolyte cell was used by Ahn et al. [5] for the investigation of superconducting oxides in the Y–Ba–Cu–O system (Fig. 3). A closed quartz reactor with two incorporated compartments was constructed. Each compartment had its own furnace for independent temperature control. The Y–Ba–Cu–O sample was placed in one compartment, and a YSZ solid electrolyte tube, closed at one end, was placed in the other compartment. The YSZ

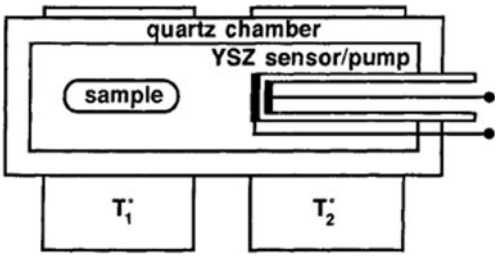

Fig. 3 Schematic view of the apparatus [5]

tube with porous platinum electrodes was periodically used as an oxygen sensor for monitoring oxygen concentration in the reactor or as an oxygen pump to quantitatively titrate oxygen into the reactor or out of it. The solid electrolyte part of the device was heated to a fixed temperature of 850 °C (T_2) separately from that of a sample which could be investigated at much lower temperature (T_1=500 °C). It was found that a $YBa_2Cu_3O_x$ material with an oxygen content below x=6.5 could be prepared at low temperature by the removal of oxygen from $YBa_2Cu_3O_7$. This technique allowed the preparation of $Y_1Ba_2Cu_3O_x$ samples with precisely controlled oxygen content in $Y_1Ba_2Cu_3O_x$ (x=6.14–6.61) and the determination of the Y–Ba–Cu–O quaternary phase diagram in the vicinity of this composition. The temperature and oxygen partial pressure were restricted only by the properties of quartz, the sealing material, and the mixed oxide investigated.

A very similar technique (Fig. 4) was used by Li et al. [6] for the investigation of Ba-ferrite ($BaFe_{12}0_{19}$). In contrast to [5], the temperatures of the sample and the solid electrolyte sensor (pump) were the same, and the oxygen partial pressure of the sample was directly measurable in the temperature range 700–1,000 °C. The YSZ tube was housed in a quartz jacket using back-to-back stainless steel high vacuum flanges. At 1,000 °C, the lower stability limit for $BaFe_{12}O_{19}$ was found to be 3.2×10^{-6} atm oxygen. This decreased to 3.4×10^{-17} atm at 700 °C. The experimental low temperature limit was restricted by the small electrochemical activity of electrodes under 700 °C.

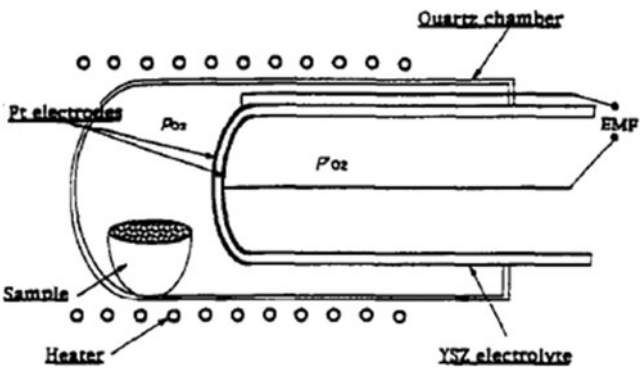

Fig. 4 Schematic of the electrochemical cell configuration used in the oxygen coulometric titration experiments [6]

p–T–x diagrams were drawn and oxygen permeability was determined for high-temperature superconducting $PrBa_2Cu_3O_{6+\delta}$ ceramic by Patrakeev et al. [7] using the cells shown in Fig. 5. In contrast to earlier cells [4, 6], two pairs of deposited platinum layers served as the oxygen sensor and pump electrodes at these measurements. The zirconia crucible was closed with a zirconia cap and sealed with an HTG for the measurement of oxygen exchange (Fig. 5a). For oxygen permeability measurements, the zirconia crucible was closed with a gas-dense $PrBa_2Cu_3O_{6+\delta}$ ceramic membrane and sealed with the same HTG (Fig. 5b). During measurements, the cells were placed in ambient air. The amounts of oxygen transported into the cell or out of it by the oxygen pumps were calculated according to Faraday's law, assuming that the oxygen transference number in zirconia is equal to unity [8].

The oxygen content isotherms for $PrBa_2Cu_3O_{6+\delta}$ were measured by coulometric titration in the temperature range 550–825 °C at oxygen partial pressures of 10^{-3} to 1 atm. The oxygen ion conductivity of the $PrBa_2Cu_3O_{6+\delta}$ compound was calculated using oxygen permeation values determined in the temperature range 600–850 °C at oxygen pressures 0.08–1.00 atm. The data were also used for the calculation of oxygen chemical diffusion coefficients. The activation energy of the oxygen conductivity and oxygen diffusivity was found to be dependent linearly on the oxygen content. The experimental temperatures (550–850 °C) and oxygen partial pressures were restricted by the properties of zirconia as a solid electrolyte, the electrode activities, and the high-temperature sealing glasses used.

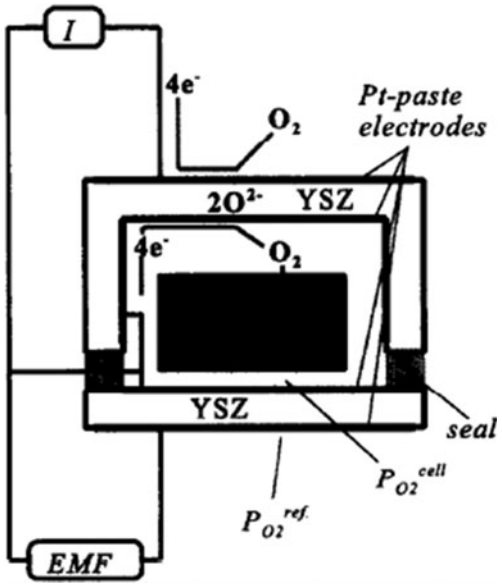

Fig. 6 Electrochemical cell used for oxygen titration experiments [9]

A similar electrochemical cell was used by Lankhorst et al. for measurements of oxygen content in $La_{0.8}Sr_{0.2}CoO_{3-\delta}$ as a function of temperature and of oxygen concentration in the gas phase [9] (Fig. 6).

The δ–pO_2 curves were measured at various temperatures by numerical integration of the current decay after a stepwise change in the cell voltage. Voltage steps of typically 25 mV were applied between 0 and 200 mV. These measurements were performed at 700, 750, 800, 850, 900, 950, and 1,000 °C. The relative positions of the resulting δ–pO_2 lines

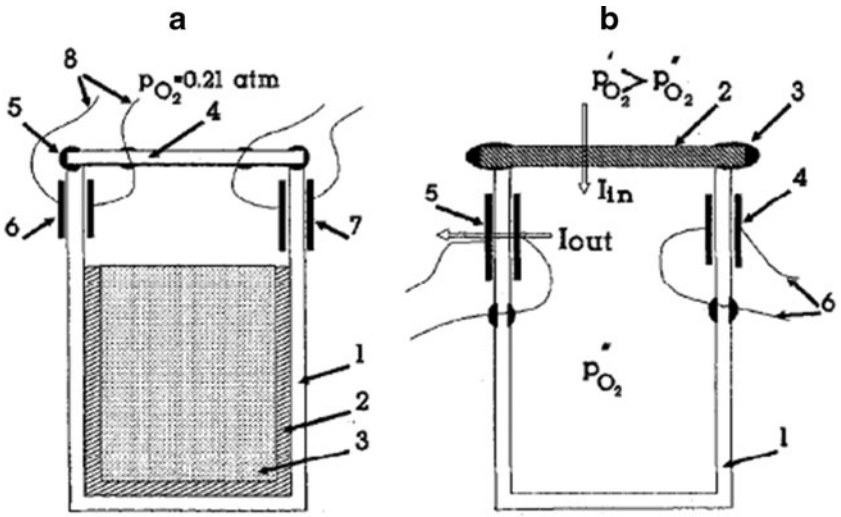

Fig. 5 Schematic representation of the electrochemical cells used for oxygen content (**a**) and oxygen permeation (**b**) coulometric measurements [7]: **a** *1* zirconia crucible, *2* corundum liner, *3* powder specimen, *4* zirconia lid, *5* HTG, *6* oxygen sensor electrodes, *7* oxygen pump electrodes, *8* voltage wires; **b** *1* zirconia crucible, *2* ceramic membrane of the specimen under experiment, *3* HTG, *4* oxygen sensor electrodes, *5* oxygen pump electrodes, *6* voltage wires, I_{in} oxygen flux into the internal space of the zirconia cell owing to the oxygen permeability of membrane 2, I_{out} oxygen flux due to voltage applied to the electrodes of pump 5

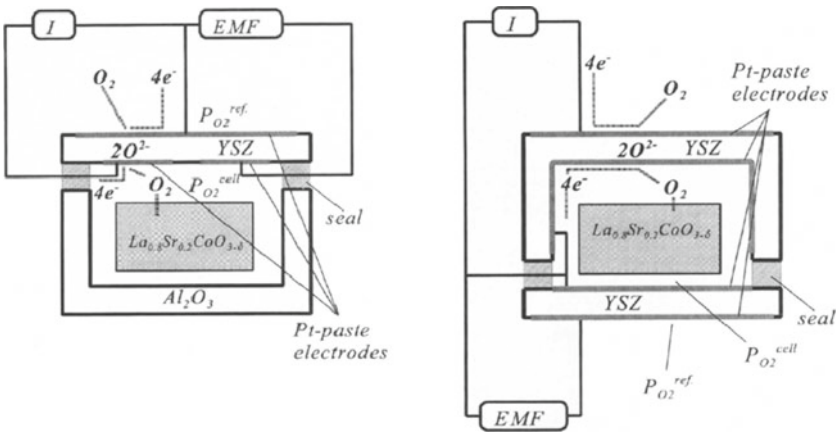

Fig. 7 Schematic diagrams of two of the electrochemical cells used for $La_{0.8}Sr_{0.2}CoO_{3-\delta}$ investigation [10]

were determined by measuring the open-circuit electromotive force (EMF) while changing the temperature. To measure the energy and entropy of oxygen incorporation, the open-circuit EMF was monitored as a function of temperature at constant oxygen nonstoichiometry. These temperature step measurements were performed in the range $0.01>\delta>0.085$. Between two temperature steps, the oxygen stoichiometry of the sample was adjusted by electrochemical pumping of oxygen into the cell or out of it.

Lankhorst and Bouwmeester [10] have investigated the same compound using the two different cells shown in Fig. 7.

The electrochemical cells used (Figs. 6 and 7) were constructed according to the cell previously described by Lade and Jacobsen [11] for the determination of chemical diffusion and oxygen exchange coefficients in mixed ionic–electronic conducting oxides. These measurements were performed after stepwise change of oxygen partial pressure in the container (Fig. 8) and showed similar results. The gold gasket in the cell [11] was then changed to a high-temperature Pyrex glass ring [9, 10]. To take into account the pO_2-dependent polarization losses at the internal YSZ/Pt/O_2 interface, the authors [9, 10] applied a reference electrode. The cell used by Lade and Jacobsen contained a reference electrode to account for the pO_2-independent polarization losses at the external YSZ/Pt/O_2 interface.

Another solid electrolyte coulometric cell was developed by Patrakeev et al. [12] for high-precision coulometric

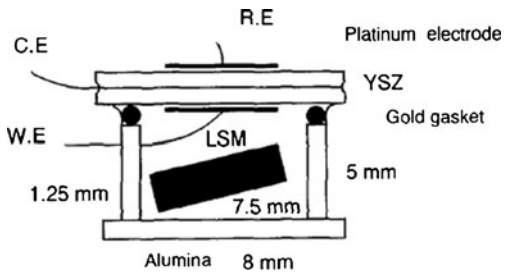

Fig. 8 Electrochemical cell: *RE* reference electrode, *WE* working electrode, *CE* solid electrolyte [11]

measurements of the equilibrium oxygen content in the $YBa_2Cu_{3-x}Co_xO_{6+\delta}$ solid solution. The authors wrote that the main uncertainty of the method in the case of the standard single cell [7, 13] was related to an uncontrollable leak of oxygen into the experimental cell resulting from the small electronic conductivity of the solid electrolyte. To minimize this bypass flux, the measuring cell was placed inside an auxiliary electrochemical cell so that it is possible to maintain a nearly zero oxygen pressure gradient across the wall of the measuring cell during experimental runs (Fig. 9). The oxygen

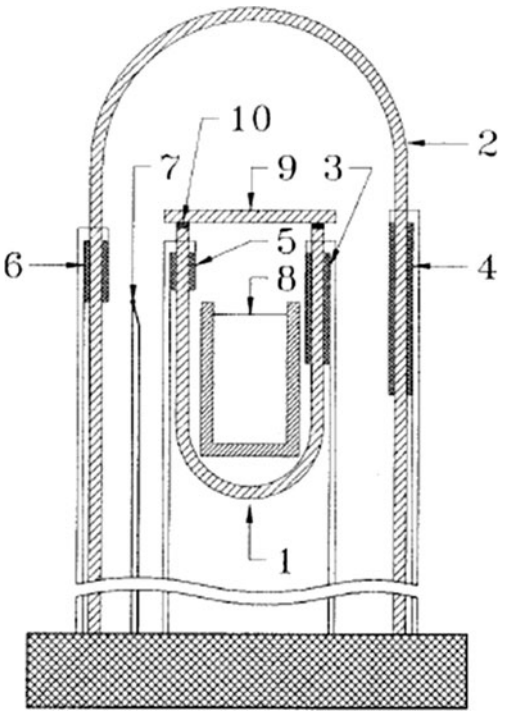

Fig. 9 Schematic drawing of the double cell for the coulometric titration (not to scale): *1* measuring cell of the $ZrO_2(Y_2O_3)$ oxygen solid electrolyte, *2* covering cell of the zirconia electrolyte, *3* and *4* oxygen pump, *5* and *6* oxygen sensor, *7* thermocouple, *8* material under study (about 200 mg), *9* zirconia lid, *10* HTG [12]

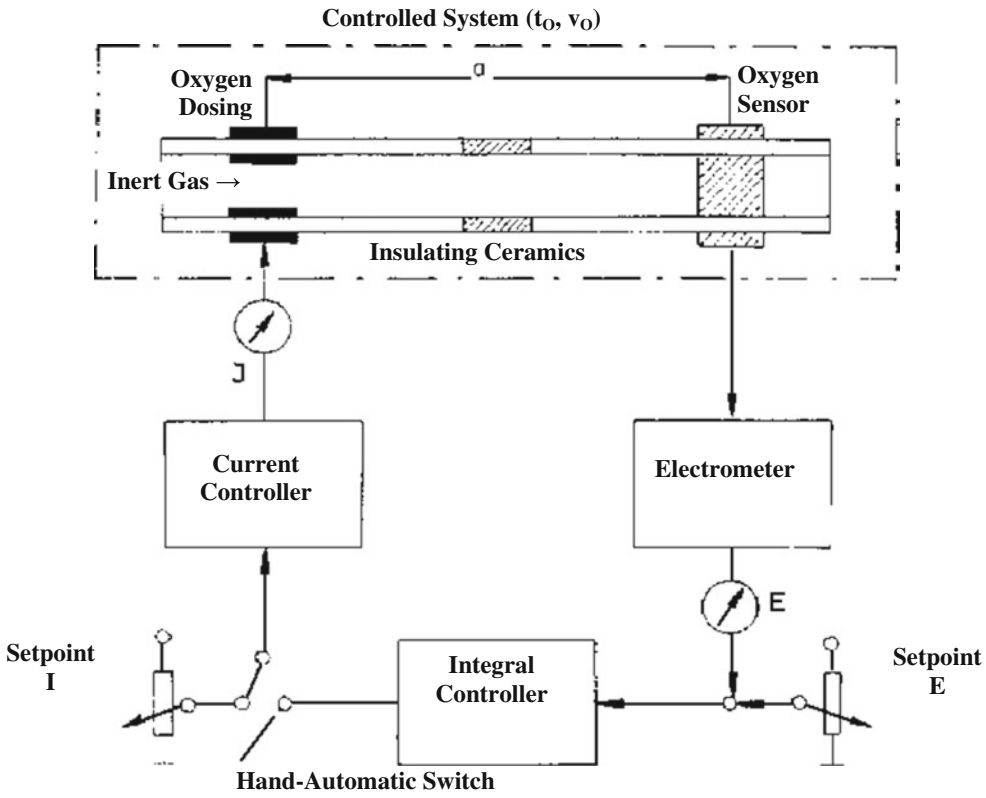

Fig. 10 Diagram of a pump–gauge measurement device [25]

pressure pO_2 in the measuring cell was calculated from the relation:

$$\log pO_2 = \frac{21.159}{T} \cdot (E_m + E_i) - 0.69 \qquad (7)$$

where E_m and E_i stand for voltage at the oxygen sensor of the measuring and isolating cell, respectively. The titration was carried out by changing the oxygen partial pressure in the measuring cell using the electrochemical pump. The oxygen pump of the isolating cell worked simultaneously to maintain a minimal voltage at the sensor of the measuring cell. The absolute value of (E_i) during experiments did not exceed 2 mV. As a result, the error in the determination of (δ) relative to the reference point did not exceed 0.002.

A four-probe arrangement was used for simultaneous measurement of the high-temperature conductivity and the thermal EMF in ceramic specimens. The measurements were carried out in the cell analogous to that depicted in Fig. 9, which enabled change and control of the oxygen pressure over the sample. The oxygen content in the specimen at a given temperature and oxygen pressure was calculated from the coulometric titration data. However, the above-mentioned restrictions of closed coulometric cells remained unavoidable in these experiments.

Oxygen solid electrolyte coulometry in open systems

According to Fouletier et al. [14], the idea of free gaseous oxygen pumping was initially suggested in the mid-1960s by Weissbart et al. [15] and Antonsen et al. [16]. The first quantitative study of this idea was performed by Bulliere [17]. In 1969, Besson et al. patented [18] the electrochemical method for separating O_2 from a gas, generating electricity and measuring the oxygen partial pressure. The proposed device provides oxygen-inert gas mixtures of

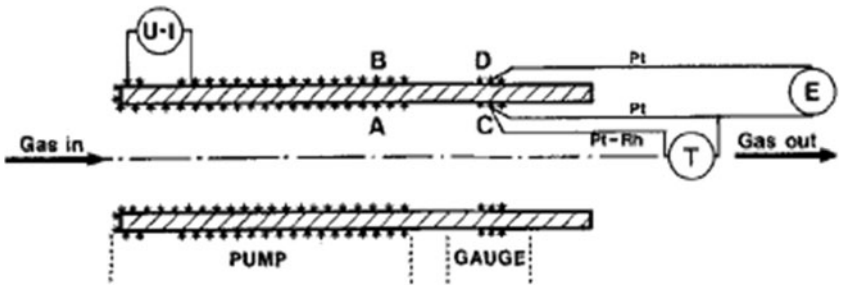

Fig. 11 Diagram of a pump–gauge cell [14]

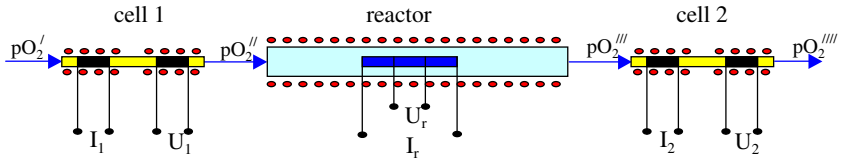

Fig. 12 Schematic of the OXYLYT™ device for simultaneous in situ OSEC and electrical conductivity measurements [26]

well-defined compositions. Beekmans and Heyne [19] developed in 1971 the electronic regulation of the pumping process, generating a constant oxygen pressure in a flowing gas carrier. Rapp [20] patented and described in detail an adequate device for oxygen pumping.

Hartung and Möbius [21] pointed out the oxygen semipermeability of the solid electrolyte tubes used, which may be considered to be a serious drawback of the proposed method, but following investigations by Beekmans et al. [19], Besson et al. [22], and Fouletier et al. [14, 23, 24], they described a pump and a gauge device, which obviate the main disadvantages of the initial designs. Physical oxygen permeability due to porosity, "electrochemical oxygen permeability" of solid electrolytes due to electronic conductivity, and temperature gradient between the working and reference electrodes could be eliminated or compensated by electronic devices.

The first practically useful oxygen pump–gauge devices for the preparation of oxygen-inert gas mixtures with well-determined compositions were developed and submitted for publication almost simultaneously in March 1975 (Figs. 10 and 11, following [25] and [14], respectively). The manuscript [25] was submitted 3 weeks earlier.

The conventional pump–gauge devices were simply metal coatings deposited on solid electrolyte tubes. YSZ or calcium-stabilized zirconia was utilized as solid electrolyte material, and Pt was utilized as electrodes. The operating temperature was between 600 and 800 °C. The analyzed gas flowed in the tubes and ambient air was in contact with the external electrodes.

A known current was passed through the electrolyte in the pump zone by applying a suitable voltage between the electrodes. If the electrolysis obeys Faraday's law, the flow of oxygen being pumped from the outside to the inside of the tubes can be easily calculated (Eqs. 1 and 2). A new apparatus using a microgauge [14] was capable of producing oxygen-inert gas mixtures with oxygen concentrations ranging down to some 10^{-2} ppm within an accuracy of a few percent.

A coulometric procedure for the determination of hydrogen in inert gases has been given [25]. Hydrogen was titrated with oxygen introduced electrochemically into the gas stream. The determination of the equivalence point followed gas potentiometrically. This procedure was used for the determination of hydrogen permeation through the walls of a nickel membrane in the temperature range 180–350 °C. The other species (CO, CH_4, and others) can also be determined with similar accuracy. In addition to its analytical use, the device is able to measure oxygen partial pressure and to prepare gas mixtures with constant oxygen concentration, which can be lower or higher than that in the input gas.

The first industrial measurement system was OXYLYT™ (SensoTech, Magdeburg, Germany) developed in the early

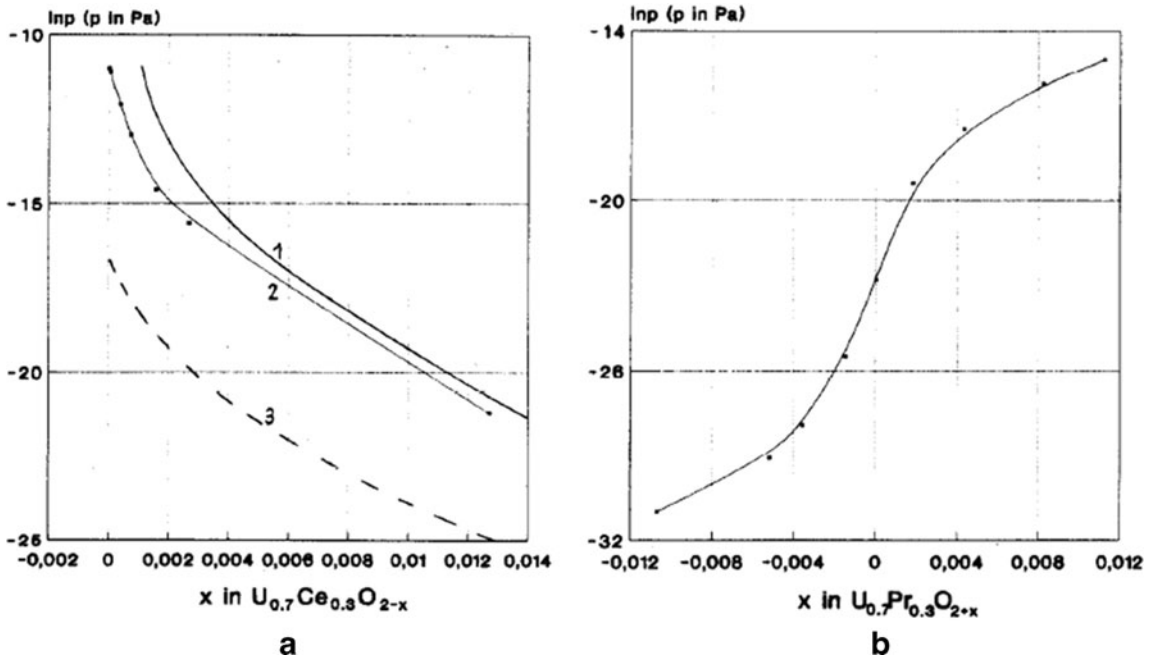

Fig. 13 Oxygen content of $U_{0.7}Ce_{0.3}O_{2-\delta}$ (**a**) and $U_{0.7}Pr_{0.3}O_{2+\delta}$ (**b**) as functions of oxygen partial pressure at 1,223 K [32, 33]

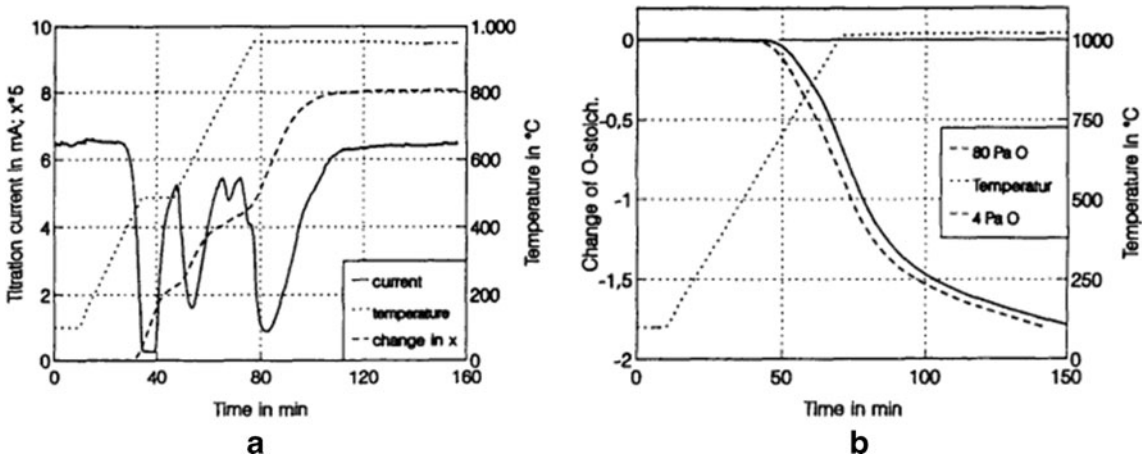

Fig. 14 OSEC measurement of oxygen exchange in $YBa_2Cu_30_{6.7}$ powder in Ar–O_2 at pO_2=24 Pa (**a**) and change of oxygen stoichiometry of YBaCuO core in an AgPd tape (**b**) [38]

1990s. It used both SEC and potentiometry methods [26]. This system operates in a carrier gas mode and has no restrictions on the measurement conditions for the samples, such as temperature or oxygen concentration. Therefore, it is more flexible in comparison with closed systems normally using the same temperature for both the solid electrolyte cell and the sample under investigation. By OSEC in open systems, materials and processes can be investigated at every temperature and atmospheres, except those combustible and aggressive to electrodes and solid electrolyte gases. Gas mixtures with small concentrations of burning gases equilibrated with oxygen under the experimental conditions (H_2O, H_2, O_2, CO_2, CO, and O_2) can also be successfully investigated by this method. Other material properties, such as electrical conductivity, magnetization, and crystal structure could be easily determined online simultaneously with oxygen exchange.

Figure 12 illustrates the operating principle of the OXYLYT™ open solid electrolyte coulometric and potentiometric system.

Two identical solid electrolyte cells are utilized in this measurement system. Each cell has a pair of oxygen pumping (*I*) and potential measurement (*U*) electrodes. The cells allow the preparation of steady-state gas flows with a given oxygen concentration by presetting the electrode voltage (*U*) at a known temperature. The voltage is controlled by feedback adjustment of the coulometric titration current (*I*) between the oxygen-pumping electrodes. If an experimental reactor with a sample is placed between two such cells, the oxygen partial pressure in the sample can vary in the range 10^{-15} to 10^5 Pa. The temperature of the reactor can be selected independently of the temperature of the pump and analyzing cells and is restricted only by the construction materials, furnace, and sample properties because the cells operate at optimum electrode and solid electrolyte conditions. Inert gases such as Ar, N_2 mixed with O_2, or gas mixtures with H_2O, H_2, O_2, CO_2, CO, and O_2, for example, may be used as carriers.

A stable oxygen partial pressure pO_2' in the inflowing gas can be modified in cell 1 by coulometric dosing with oxygen to

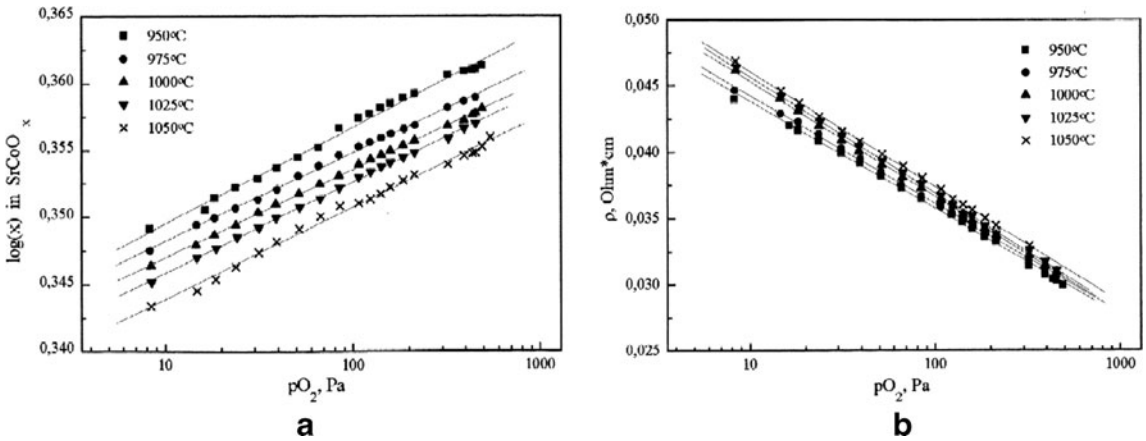

Fig. 15 Oxygen content (**a**) and resistivity (**b**) in $SrCoO_{3-x}$ versus oxygen partial pressure at different temperatures [45]

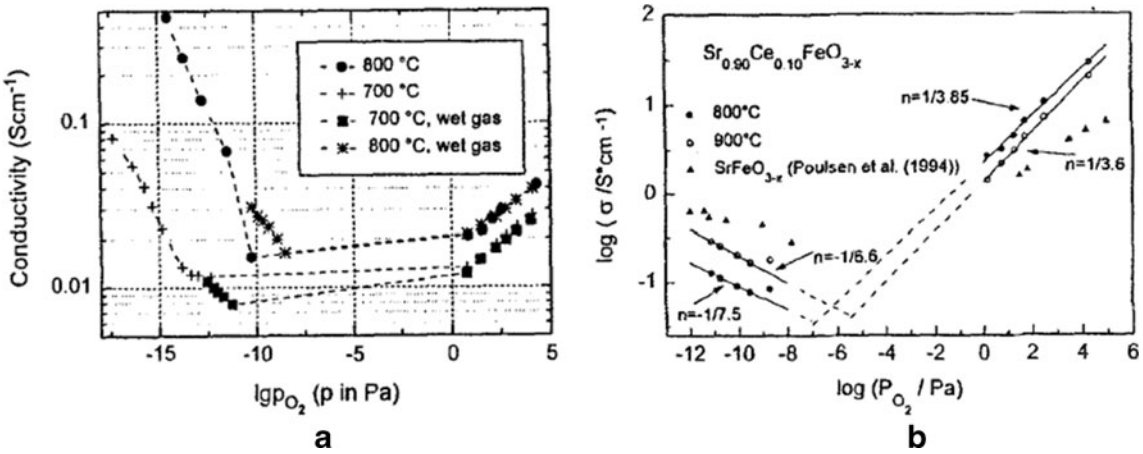

Fig. 16 Specific electrical conductivity of $Ce_{0.8}Pr_{0.2}O_{\gamma-\delta}$ (**a**) and $Sr_{0.9}Ce_{0.1}FeO_{3-\delta}$ (**b**) as a function of oxygen partial pressure [46, 47]

give the required pO_2'' values. No change of oxygen concentration in the reactor is observed if no oxygen exchange processes take place in the reactor ($pO_2''=pO_2'''$). A constant basic oxygen dosing current ($I_{2,base}$) may occur inside cell 2 if the given constant voltage (U_2) is lower than (U_1) ($pO_2''<pO_2'''$). After a sufficiently long sweep time, all controlled electrochemical parameters (I_1, I_2, U_1, and U_2) reach constant values if the gas separators are dense, the carrier gas flow is constant, and no oxygen exchange processes take place in the reactor. All oxygen exchange in the reactor should then be accompanied by a deviation of the coulometric titration current (I_2) from the ($I_{2,base}$) value, if (U_2) is kept constant. The mass of oxygen exchanged (Δm_{O_2}) may be calculated from Faraday's law:

$$\Delta m_{O_2} = \frac{M_{O_2}}{F \times z} \times \int_{t=start}^{t=end} \left(I_{2,base} - I_t\right) dt$$

$$= \frac{32}{96,500 \times 4} \times \int_{t=start}^{t=end} \left(I_{2,base} - I_t\right) dt \qquad (8)$$

Knowing the mass and chemical composition of the sample investigated, the so-called oxide p–T–x and p–T–σ diagrams are readily constructed by stepwise changing of the oxygen partial pressure and temperature in the reactor.

Some applications of OXYLYT™ and ZIROX™ devices

Many investigations were performed during the development of the OXYLYT™ prototype. Using uranium oxides as examples, Teske et al. [27] described the qualification and limitations of the SEC method. The OSEC open system method has shown higher accuracy in comparison with solid electrolyte potentiometry and does not require calibration. Standard deviations for oxygen/metal ratios down to ±0.0007 have been attained. The method showed good agreement with thermogravimetric determination of oxygen content in uranium oxides and was recommended for the preparation of nuclear fuel oxides with predetermined oxygen content. The accuracy attained in the OSEC method was confirmed by investigation

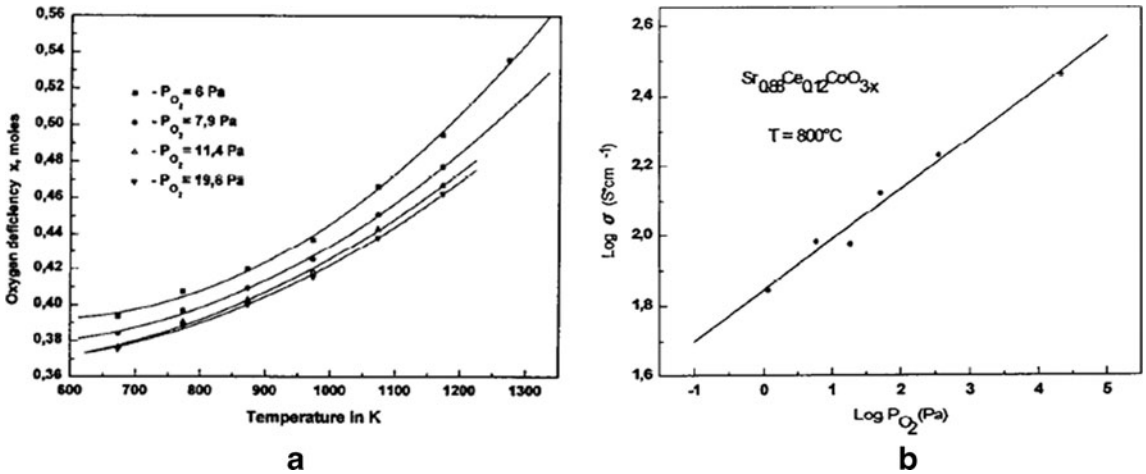

Fig. 17 Temperature dependency of oxygen deficiency (x) in $Sr_{0.85}Ce_{0.15}CoO_{3-\delta}$ at different oxygen pressures (**a**) and electrical conductivity of $Sr_{0.88}Ce_{0.12}CoO_{3-\delta}$ at 800 °C as a function of oxygen pressure (**b**) [48]

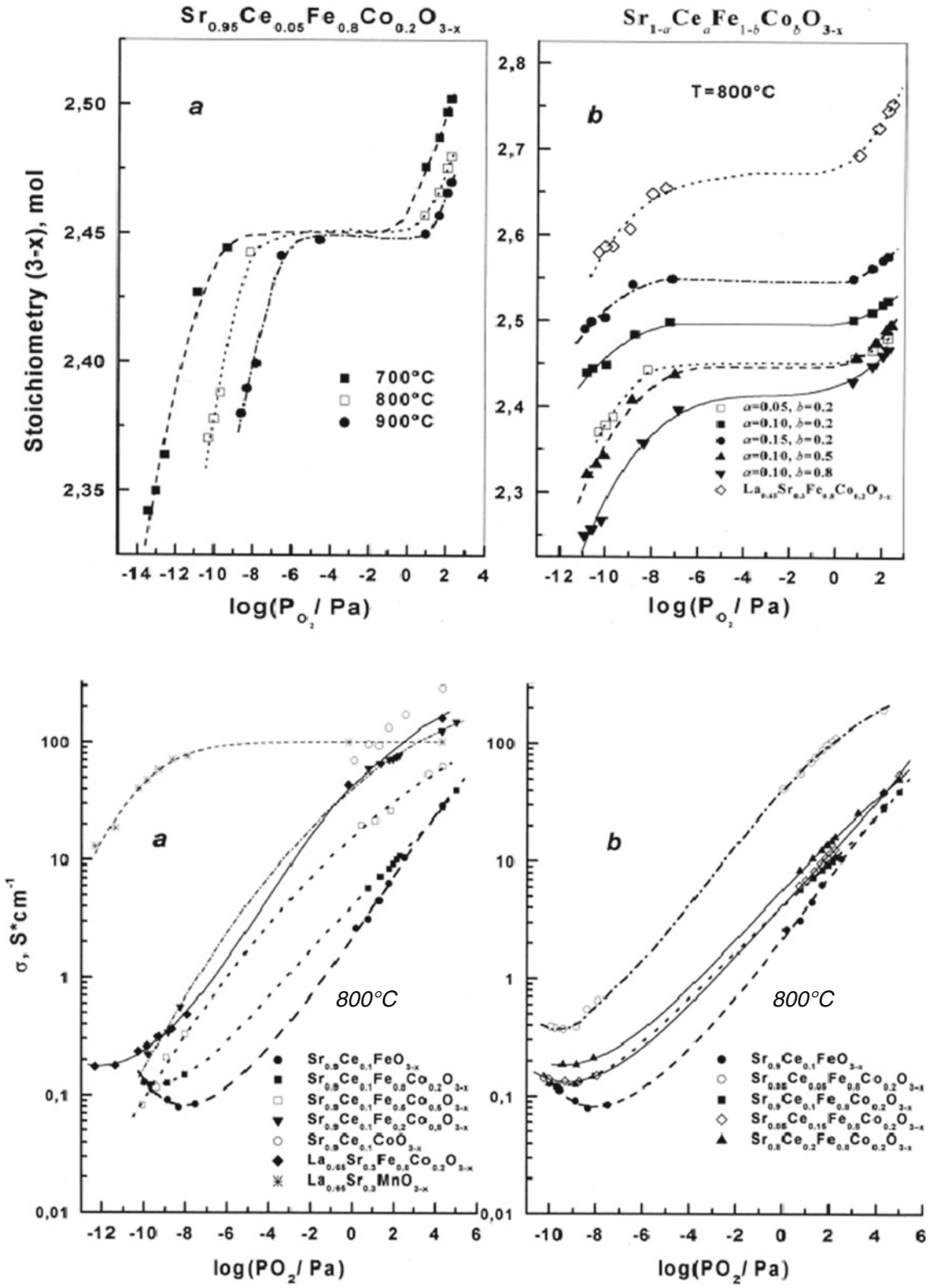

Fig. 18 Oxygen stoichiometry (*above*) and electrical conductivity of some perovskite structure compositions in the system Sr–Ce–Fe–Co–O versus oxygen partial pressure [49]

of interactions between nonstoichiometric oxides, such as CeO_{2-x}, $PrO_{1.5+\delta}$, $U_{0.7}Ce_{0.3}O_{2\pm\delta}$, $U_{0.7}Pr_{0.3}O_{2\pm\delta}$, $U_{0.8}Gd_{0.2}O_{2-\delta}$, and $U_{1-z}Pu_zO_{2+\delta}$, in ($Ar+O_2+H_2+H_2O$) gas mixtures at 1,050–1,350 K [28, 29].

Table 1 Oxygen nonstoichiometry, δ, of $MnFe_2O_{4+\delta}$ samples [51]

Point	Atmosphere	$Log\, pO_2$ (atm)	Temperature in °C	δ in $MnFe_2O_{4+\delta}$
1	$Ar/H_2O/H_2$	−19.2	600	δ_1=−0.013
2	$Ar/H_2O/H_2$	−16.2	700	δ_1=−0.026
3	Ar	−4.6	700	δ_1=0.014
4	Ar	−4.6	800	δ_1=0.007
5	Ar/O_2	−3.8	550	δ_1=0.180
6	Air	−0.68	400	δ_1=0.420

The applicability of solid electrolyte coulometric cells as gas chromatography detectors (GCD) has been successfully demonstrated [30]. The concept was to use the coulometrically generated oxygen in a feedback fashion, thereby generating a detector signal corresponding to oxygen consumption. A solid electrolyte tube with a pair of oxygen sensors at the pumping input and output was used as a GCD in the output gas line from the gas chromatography column. Testing of this detector showed that oxygen, hydrogen, nitrogen oxides, and hydrocarbons such as methane, ethane, propane, and butane can be detected into the parts per billion region (10^{-9}) in gas mixtures with inert gases.

Since the end of the 1980s, over 50 papers describing measurements using OXYLYT™ and its successors produced by ZIROX™ (Greifswald, Germany) have been published.

The general reaction $U_yMe_{1-y}O_{2+x}+\delta H_2=U_yMe_{1-y}O_{2+x-\delta}+\delta H_2O$ (Me=Pu, rare earths) has been investigated using a solid electrolyte-based coulometric technique in a carrier gas mode. The changes in the hydrogen and the oxygen concentrations in the gas phase during the reaction were registered continuously by coulometric titration and potentiometric measurements. Figure 13 illustrates the pO_2 dependencies of oxygen stoichiometry indexes of $U_{0.7}Ce_{0.3}O_{2-\delta}$ (a) and $U_{0.7}Pr_{0.3}O_{2+\delta}$ (b) determined by SEC at 1,223 K as an example [31]. Lines 1 and 3 in Fig. 13a present the data [32] for comparison. Pure $UO_{1.98}$ was prepared by the coulometry method in the temperature range 500–1,200 K, its composition being then fixed by quenching to room temperature [33]

A correlation between the oxide ion conductivity and the grain boundary area of $Ce_{1-n}La_nO_{2-0.5n}$ ceramics was found by utilization of an OXYLYT™ device [34]. The grain boundaries seem to be able to participate in oxygen exchange between the polycrystalline mixed oxide and the gas phase. Their electrical conductivity was considered as predominant because the volume fraction of the grain boundaries amounts to 6 % at a grain size of 1 mm and a grain boundary thickness of approximately 30 nm.

Low oxygen deficiency was detected by coulometry in $ZnO_{1-\delta}$ [35]. At 1,373 K, solid solution exists up to x=0.002.

OSEC may be used for measuring oxygen concentrations in the few parts per million to several percent range if a diffusion barrier on the cathode side of a ZrO_2-based solid electrolyte cell is provided. If a voltage U is applied to such a diffusion-controlled sensor device, the current in this circuit is proportional to the oxygen concentration. The necessary components of the pumping voltage control have been developed and described [36].

Oxygen exchange between mixed oxides of the Y–Ba–Cu–O system and the gas phase was investigated under reduced oxygen pressure by a solid electrolyte-based coulometric technique in a carrier gas mode [37–41] As an example, Fig. 14 shows some data for heat-treated $YBa_2Cu_3O_{6.7}$

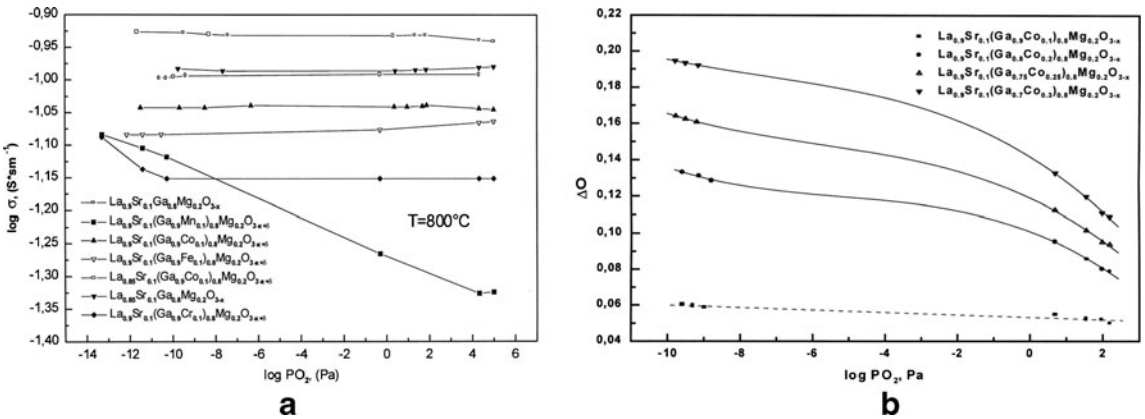

Fig. 19 pO_2 dependencies of conductivity (**a**) and amount of desorbed oxygen from air-oxidized $La_{0.9}Sr_{0.1}(Ga_{1-y}M_y)_{0.8}Mg_{0.2}O_{3-x}$ samples (**b**) at 800 °C [57]

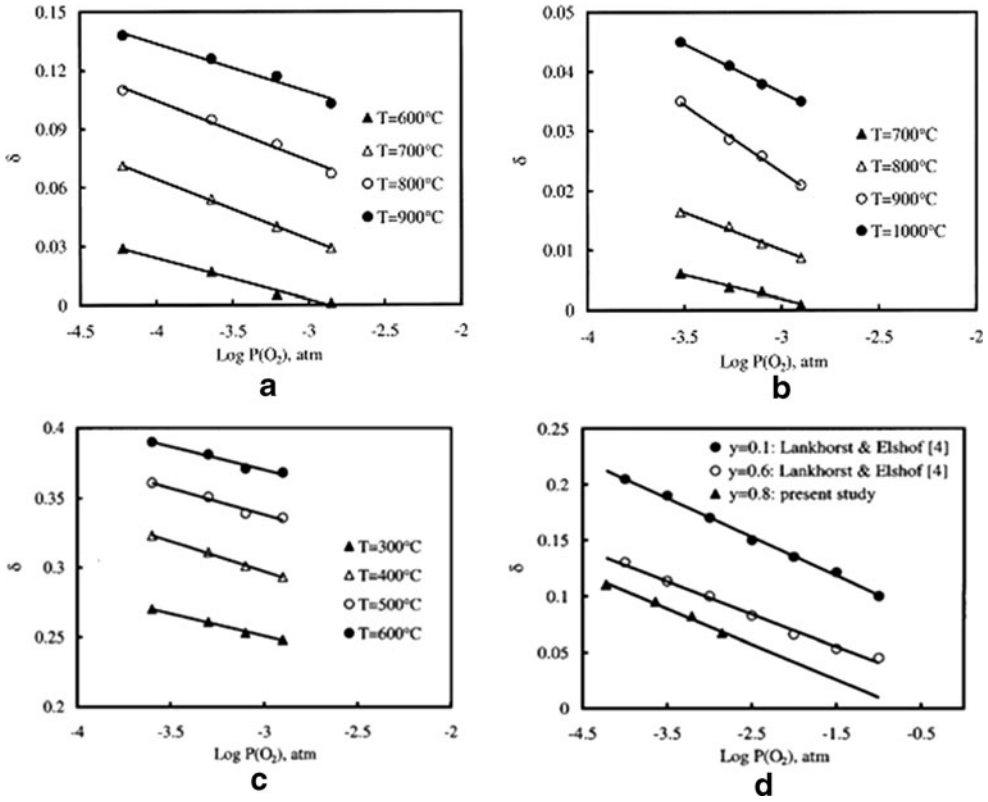

Fig. 20 Oxygen nonstoichiometry as a function of pO_2 for LSCF 6428 (**a**) LSCF 8228 (**b**), and LSCF 2882 (**c**) at different temperatures and for various $La_{0.6}Sr_{0.4}Co_{1-y}Fe_yO_{3-\delta}$ (**d**) at 800 °C ([62, 63], *4* denotes [101])

powder and high-temperature superconductor cores in AgPd-sheathed tapes [38]. Oxygen release from YBaCuO core tape during heating to 1,000 °C in an oxygen-poor atmosphere was characterized by the decreasing oxygen atomic stoichiometry index of $YBa_2Cu_3O_{6.7}$ of up to 4.7.

Heating of the $Nd_{2-x}Ce_xCuO_\psi$ single crystal, with a constant Ar flow rate at pO_2=100 Pa, is accompanied by two oxygen desorption rate maxima at 923–1,173 K [42, 43]. These are probably connected with desorption of oxygen from different crystallographic positions in the compounds. Distortions of the crystal lattice are likely caused not only by variation of its oxygen content, which may be reduced from 4.00 to as small as 3.94, but also by oxygen redistribution between crystallographic positions 02 and 01. Using the SEC technique, a three-step reduction process of thick superconducting $Nd_{2-x}Ce_xCuO_\psi$ ($0<x<0.17$) single crystals of perfect quality with a critical temperature T_c=19 K was developed [42, 43].

For analytical control, the Ti^{3+} content of the $Li_{1-x}Mg_xTi^{III}{}_{1+x}Ti^{IV}{}_{1-x}O_4$ samples prepared was determined by solid-state coulometric titration using an OXYLYT™ apparatus [44].

Strontium cobaltite $SrCoO_{3-\delta}$ was investigated using SEC and resistivity measurements in the temperature range 20–1,050 °C under oxygen partial pressures of 0.5–400 Pa [45]. It was found that two observed oxygen desorption/sorption maxima within the temperature range 500–950 °C correlated with phase transitions, as had been previously

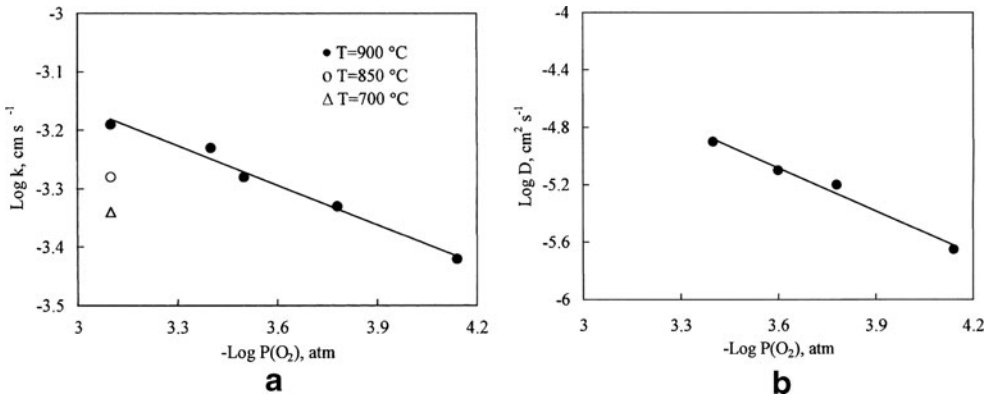

Fig. 21 log(*k*) at various temperatures (**a**) and log(*D*) at 900 °C (**b**) as functions of log (pO_2) for powdered $La_{0.6}Sr_{0.4}Co_{0.2}Fe_{0.8}O_{3-\delta}$ [60]

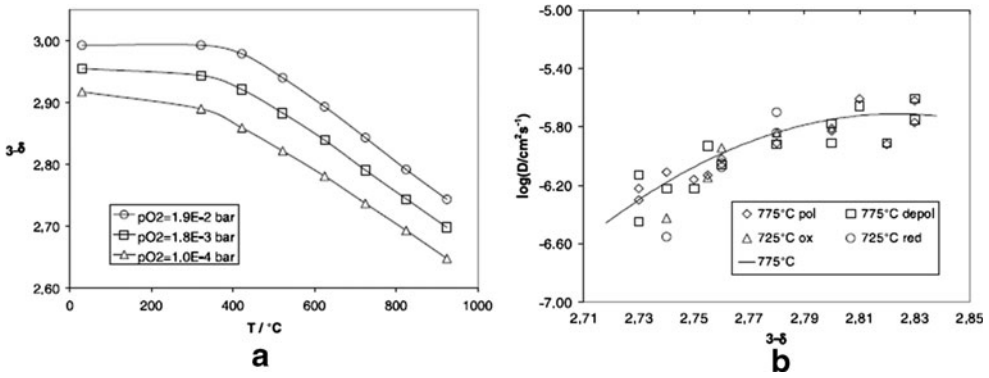

Fig. 22 Oxygen stoichiometry as a function of temperature at various oxygen partial pressures (**a**) and chemical diffusion coefficient D of $La_{0.4}Sr_{0.6}CoO_{3-\delta}$ as a function of the oxygen stoichiometry at 725 °C from oxygen exchange experiments (*ox* oxidation, *red* reduction) and at 775 °C from galvanostatic polarization measurements (*pol* polarization, *depol* depolarization) (**b**) [66]

reported in the literature. An additional oxygen desorption/sorption maximum was found at temperatures of 965–1,000 °C, which was explained as an order–disorder transition of the cubic high-temperature phase. The dependencies of the equilibrium values of oxygen content as well as specific resistivity on temperature and oxygen partial pressure were determined for the cubic phase (Fig. 15).

The OSEC was directly coupled with electrical conductivity measurements [46]. It was found that the oxidation state of Pr in the fluorite-type phases increases from $PrO_{2-\delta}$ to $Ce_{0.8}Pr_{0.2}O_{\psi-\delta}$ and to $Ce_{0.8}Sr_{0.08}Pr_{0.12}O_{\psi-\delta}$ and that the conductivities of these oxides increase with the Pr oxidation state. Changing from n-type to p-type conductivity was observed with increasing oxygen concentration in the gas phase for both $Ce_{0.8}Pr_{0.2}O_{\psi-\delta}$ (Fig. 16a) and $Ce_{0.8}Sr_{0.08}Pr_{0.12}O_{\psi-\delta}$ at $pO_2 = 10^{-10}$ to 1 Pa at temperatures of 700–800 °C. A similar conductivity behavior (Fig. 16b) was also observed in $Sr_{0.9}Ce_{0.1}FeO_{3-\delta}$ at $pO_2 = 10^{-7}$ and 10^{-5} Pa at 800 and 900 °C, respectively [46, 47]. In temperature-programmed plots for $Sr_{1-y}Ce_yFeO_{3-\delta}$ solid solutions, the oxygen release maxima were found, which pointed to possible phase transitions in these perovskite-type compounds.

The p–T–x and p–T–σ diagrams were established for some cobaltites in the $Sr_{1-y}Ce_yCoO_{3-\delta}$ system [48], analogous to the above-mentioned $Sr_{1-y}Ce_yFeO_{3-\delta}$. Oxygen deficiency x of $Sr_{0.85}Ce_{0.15}CoO_{3-\delta}$ was found to change between 0.37 and 0.55, depending on temperature (400–1,000 °C) and oxygen partial pressure varying from 6 to 20 Pa (Fig. 17a). The $Sr_{0.88}Ce_{0.12}CoO_{3-\delta}$ composition showed p-type semiconductivity at 800 °C with pO_2 in the range 0.1–10^5 Pa (Fig. 17b). In air, the maximum conductivity of 500 S/cm was found at 400 °C for y=0.15.

Oxygen stoichiometry and total and ionic conductivities of some compositions in the $Sr_{1-x}Ce_xFe_{1-y}Co_yO_{3-\delta}$ (x=0–0.2, y=0–1.0) system have been investigated (Fig. 18) [49]. The oxygen deficiencies increase with decreasing pO_2, increasing cobalt content, and decreasing ceria content at $pO_2 = 10^{-14}$ to 10^2 Pa at 700–800 °C. In compositions with high Co content, additional phases resulting from decomposition such as SrO, CeO_2, Fe_2O_3, and CoO or metallic cobalt occur below 10^{-10} Pa.

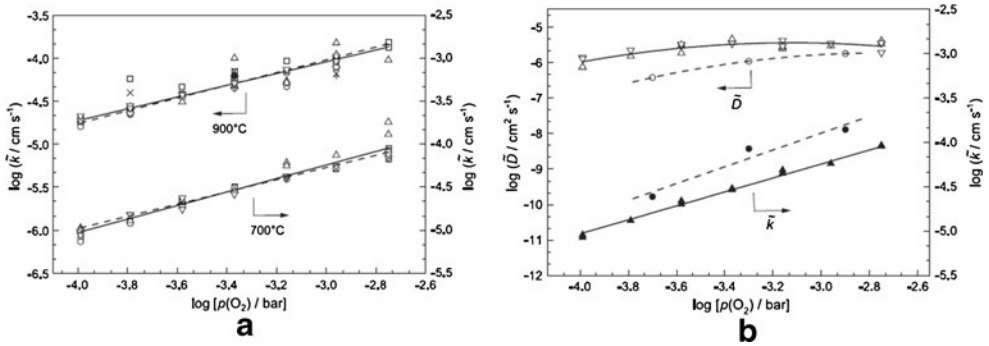

Fig. 23 Log–log plots of the surface exchange coefficient of $La_{0.4}Sr_{0.6}FeO_{3-\delta}$ at 700 and 900 °C (**a**) and of the chemical diffusion and surface exchange coefficients versus oxygen partial pressure (**b**) determined by different methods at 700–725 °C [68]: carrier gas coulometry: *inverted open triangles* and *plus sign* reduction, *open circles* and *open diamonds* oxidation; conductivity relaxation: *open triangles* and *multiplication sign* reduction, *open squares* and *filled diamonds* oxidation

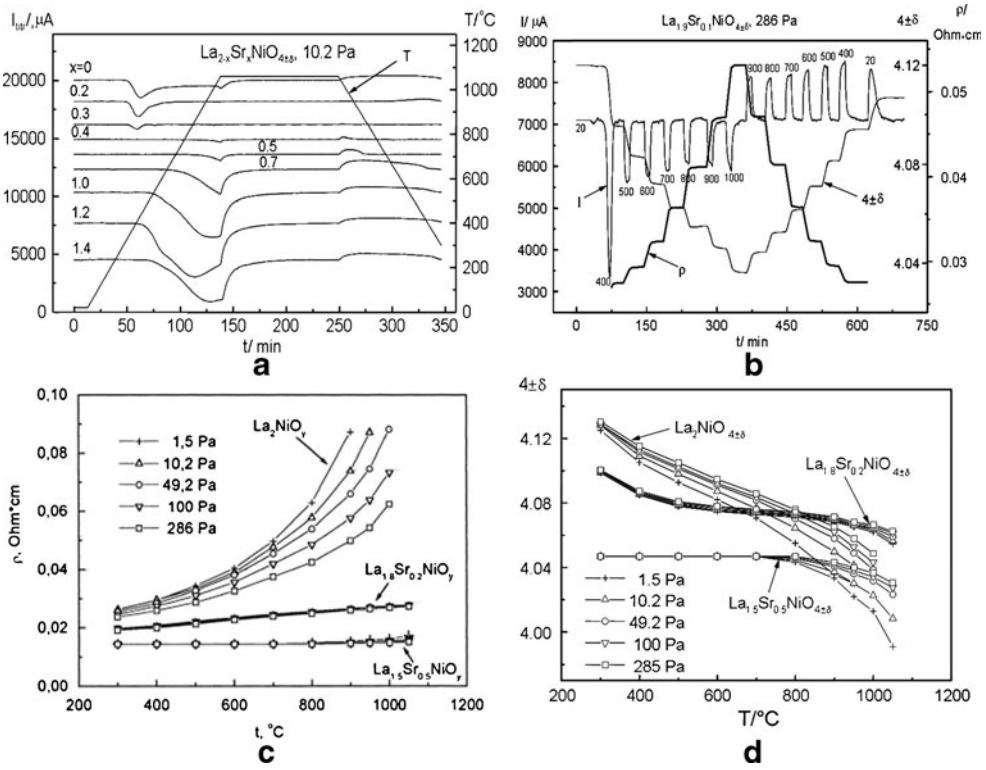

Fig. 24 Temperature dependences of titration current in a coulometric cell (**a**), oxygen content and resistance (**b**), resistance (**c**), and oxygen content (**d**) in some $La_{2-x}Sr_xNiO_{4\pm\delta}$ ceramics in Ar/O_2 gas flows at different oxygen concentrations [70, 73]

The O/Mn ratio of $MnO_{1+\delta}$ crystals prepared by the chemical transport reaction with HCl was determined by the SEC using an OXYLYT™ device [50]. It was found that y values in $MnO_{1+\delta}$ change with deposition temperature from 0.0025 at 1,091 K to 0.0128 at 1,292 K.

The phase stability and oxygen stoichiometry of manganese ferrite $MnFe_2O_{4+\delta}$ were investigated at 400–900 °C as a function of oxygen partial pressure [51]. Oxygen nonstoichiometry, δ, determined by a solid electrolyte-based coulometric technique in differently prepared samples is given in Table 1.

SEC, together with thermogravimetric analysis and X-ray diffraction (XRD), was used to examine the stable phases in the Li–Mn–O system [52]. It was found that, between 400 and 880 °C, only a spinel with the composition $Li_{1+x}Mn_{2-x}O_{4+\delta}$ ($\delta\approx0$) is stable. The lithium nonstoichiometry, x, is a function of temperature and oxygen partial pressure. The value of x increases with decreasing temperature and increasing pO_2. The possible lithium stoichiometry range Δx at a given temperature and oxygen partial pressure is much smaller than previously accepted. It was found that $0.05<\Delta x<0.13$. The spinel $Li_{1+x}Mn_{2-x}O_{4+\delta}$ has a negligible oxygen nonstoichiometric range, $\delta<0.02$. Below 400 °C, it appears to be stable only as $Li_4Mn_5O_{12}$ and $LiMn_{1.75}O_4$.

Künstler et al. [53] had investigated the oxygen exchange of $BaCe_{0.8}In_{0.2}O_{3-\alpha-y}$ as a potential solid electrolyte. For the determination of the amount of exchanged oxygen, the pulverized material was annealed between 100 and 900 °C in a gas stream with a $pH_2O/pH_2=15$ and quenched afterwards. The amount of oxygen exchanged with the sample was determined by the oxygen partial pressure change in a nitrogen carrier gas at $pO_2=0.2$ Pa by means of coulometric titration. It was found that the exchanged oxygen increased with the

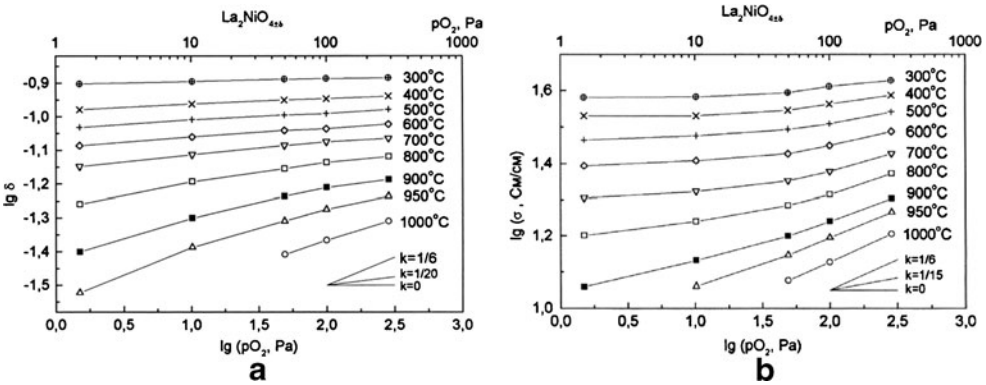

Fig. 25 Oxygen nonstoichiometry (**a**) and specific resistance (**b**) versus oxygen pressure at different temperatures for $La_2NiO_{4\pm\delta}$ [71]

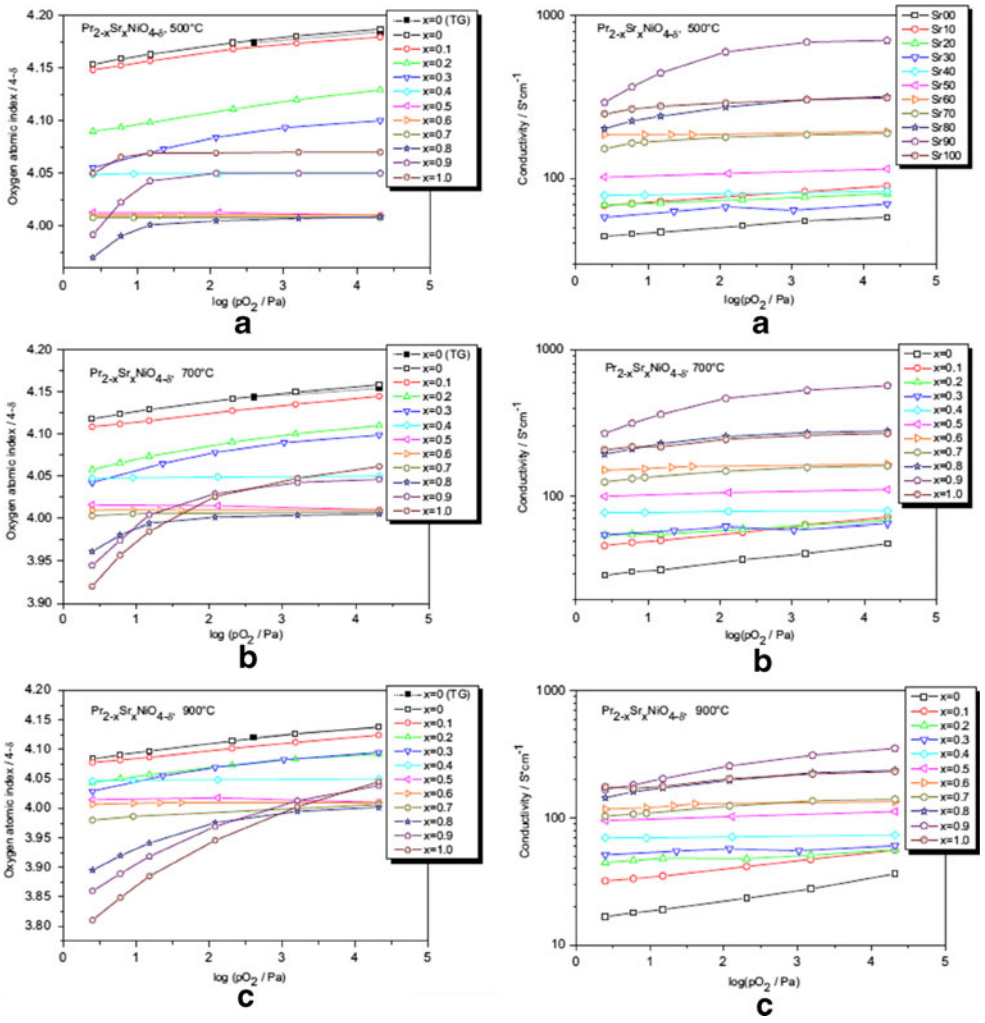

Fig. 26 The pO_2 dependencies of oxygen content (*left*) and electrical conductivity (*right*) of the $Pr_{2-x}Sr_xNiO_{4\pm\delta}$ series with x=0–1.0 determined by SEC at 500 °C (**a**), 700 °C (**b**), and 900 °C (**c**) [76]

temperature following the equation $\log y = -(4.09\pm0.09) - (1{,}170\pm60)/T$, where y is the amount of exchanged oxygen in moles per gram of sample. The minimum temperature for the absorption of oxygen into the crystal lattice was about 200 °C.

Reduction stability of $Ln_2Ni_{0.8}Cu_{0.2}O_4$ (Ln=La, Pr, Nd) compositions with K_2NiF_4-type structure in nitrogen as well as in a reducing atmosphere and their oxygen permeability under an air–nitrogen/oxygen partial pressure gradient has been investigated [54]. It was found that the compositions with Ln=La and Pr were stable in nitrogen (T=950 °C), whereas the composition with Ln=Nd showed partial decomposition. The assumption that the decrease of stability to reduction depends on the increasing atomic number of the rare earth

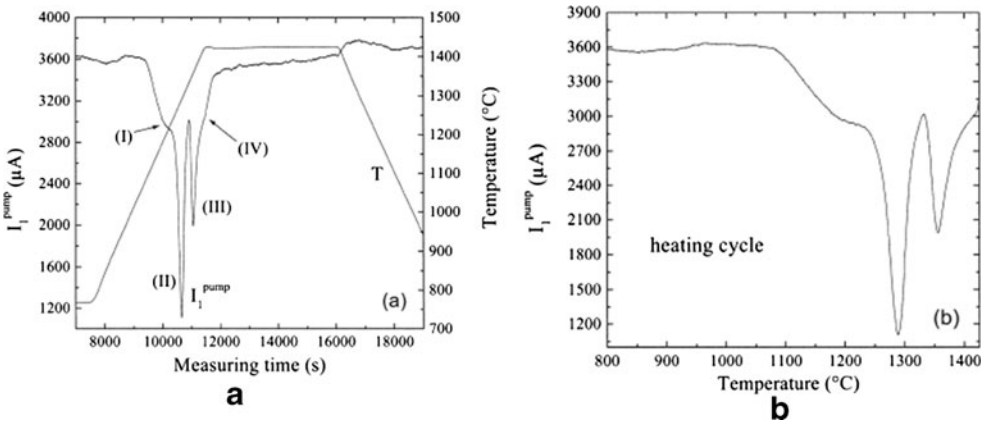

Fig. 27 Dependence of pumping current on both time (**a**) and temperature (**b**) in the coulometry cell during the sintering of a sample with 0.5 mol% La and 1 mol% excess TiO_2. Ambient atmosphere, pO_2=2.4 Pa [78, 79]

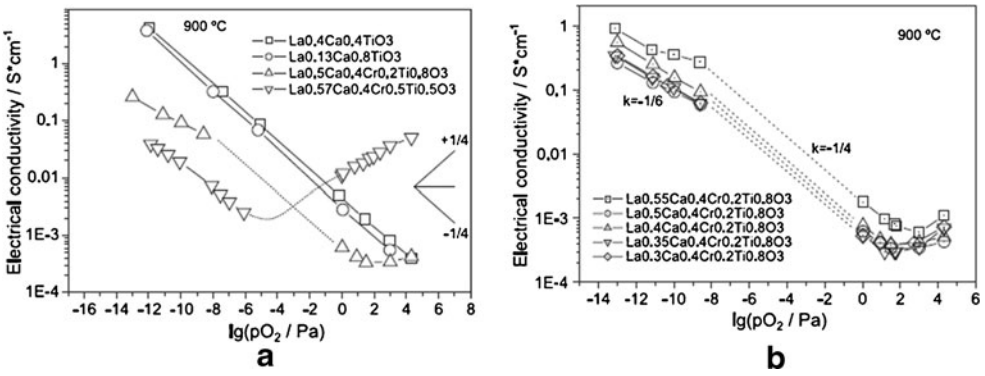

Fig. 28 Electrical conductivity as a function of oxygen partial pressure for some ceramics in the $(La_{1-x}Ca_x)_{1-\alpha}Cr_{1-y}TiyO_3$ (**a**) and $La_{0.6-\gamma}Ca_{0.4}Cr_{0.2}Ti_{0.8}O_3$ (**b**) systems at 900 °C [85]

cation was further confirmed by SEC measurements. The measured oxygen permeabilities of $Ln_2Ni_{0.8}Cu_{0.2}O_4$ changed with Ln cation in the order La<Pr<Nd (La=La, Pr, Nd, etc.).

Trofimenko and Ullmann [55, 56] and later Khorkounov [57] investigated solid solutions of lanthanum gallate, $LaGaO_3$, partially substituted by transition metals. Figure 19a illustrates that Co-substituted $La_{0.9}Sr_{0.1}(Ga_{1-y}M_y)_{0.8}Mg_{0.2}O_{3-\delta}$ compositions show the highest conductivity, and their oxygen exchange increased with Co content in the pO_2 range 10^{-10} to 100 Pa at 400–900 °C (Fig. 19b). The oxygen permeation measurements carried out with an OXYLYT™ device show an increasing hole conductivity of $La_{1-x}Sr_xGa_{1-y-z}Mg_yCo_zO_{3\pm\delta}$ with increasing Co content which provides no possibility of using these solid solutions as solid electrolytes [57].

The conductivity in two orthogonal directions of the single crystals $La_{0.95}Sr_{0.05}Ga_{0.9}Mg_{0.1}O_{2.92}$ and $La_{0.9}Sr_{0.1}Ga_{0.8}Mg_{0.2}O_{2.85}$ has been studied [58]. Both the conductivity and the structural data indicated three-phase transitions in $La_{0.95}Sr_{0.05}Ga_{0.9}Mg_{0.1}O_{2.92}$ at 520–570 K (*Imma–I2/a*), at 770 K (*I2/a–R3c*), and at 870 K (*R3c–R-3c*), respectively. Two transitions at 770 K (*I2/a–R3c*) and in the range 870–970 K (*R3c–R-3c*) occur in $La_{0.9}Sr_{0.1}Ga_{0.8}Mg_{0.2}O_{2.85}$.

Many investigations of oxygen nonstoichiometry, oxygen diffusion mobility, oxygen surface exchange, and electrical conductivity in the $La_{1-x}Sr_xCo_{1-y}Fe_yO_{3-\delta}$ system have been carried out using OSEC [59–68]. Figure 20 illustrates the oxygen nonstoichiometry index (δ) found for some compositions in this series versus oxygen concentration at different temperatures. The degree of oxygen nonstoichiometry (δ) increased with increasing temperature, decreasing oxygen partial pressure, and increasing Sr or Co content.

Relaxation experiments, following small increments in temperature or oxygen pressure, were carried out to investigate oxygen transport and surface absorption kinetics [60]. Using a suitable diffusion model and nonlinear parameter optimization, the surface exchange coefficient (k) and chemical diffusion coefficients (D) of oxygen were obtained from the experiments. The results were found to be consistent with those of other relaxation techniques.

The surface exchange and chemical diffusion coefficients were found for powdered $La_{0.6}Sr_{0.4}Co_{0.2}Fe_{0.8}O_{3-\delta}$ oxide materials at 700–900 °C and reduced oxygen pressures in the range 1×10^{-3} to 6.3×10^{-5} atm (Fig. 21). The results obtained in this study were found to be consistent with those obtained by means of other relaxation techniques.

Sitte et al. [65–68] have investigated oxygen nonstoichiometry, oxygen diffusion mobility, oxygen exchange kinetics, and oxygen ionic and total conductivity of two $La_{0.6}Sr_{0.4}CoO_{3-\delta}$ and $La_{0.4}Sr_{0.6}CoO_{3-\delta}$ compounds. Oxygen stoichiometry ($3-\delta$) of $La_{0.4}Sr_{0.6}CoO_{3-\delta}$ varied between 3.0 and 2.65 at 20–950 °C in the pO_2 range of 1×10^{-4} to 1.9×10^{-9} Pa (Fig. 22a). Chemical diffusion coefficients were found to increase with oxygen content ($3-\delta$) from 3×10^{-7} to 1.6×10^{-6} cm^2s^{-1} at 725–775 °C (Fig. 22b).

Figure 23 presents the pO_2 dependencies of oxygen exchange and oxygen chemical diffusion coefficients of

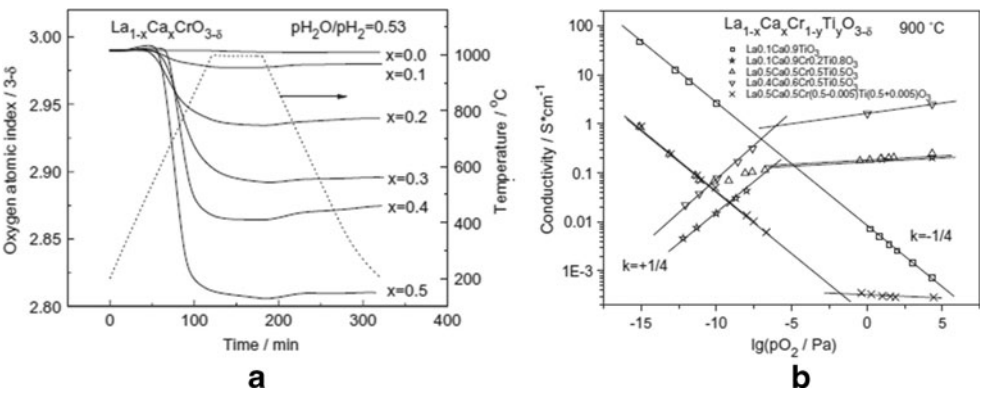

Fig. 29 Oxygen exchange of the powder samples $La_{1-x}Ca_xCrO_{3-\delta}$ during treatment under $Ar/H_2/H_2O$ gas flow and pO_2 dependence of conductivity for some ceramics in the system $La_{1-x}Ca_xCr_{1-y}Ti_yO_{3-\delta}$ at 900 °C [87]

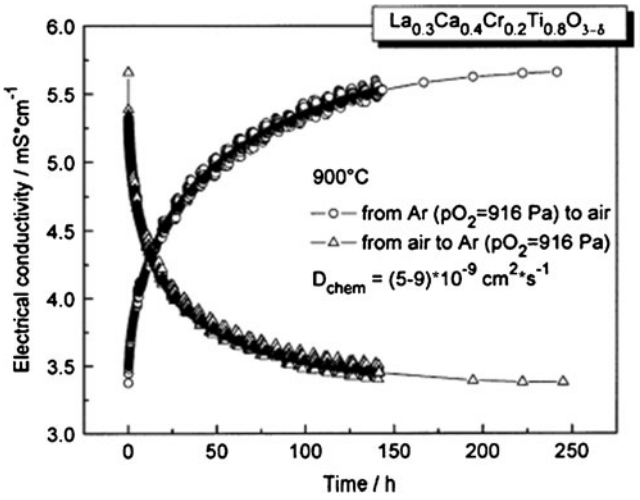

Fig. 30 Conductivity of gas-dense $La_{0.47}Ca_{0.4}Cr_{0.2}Ti_{0.8}O_{3-\delta}$ ceramic sample after corresponding gas flow switch [88]

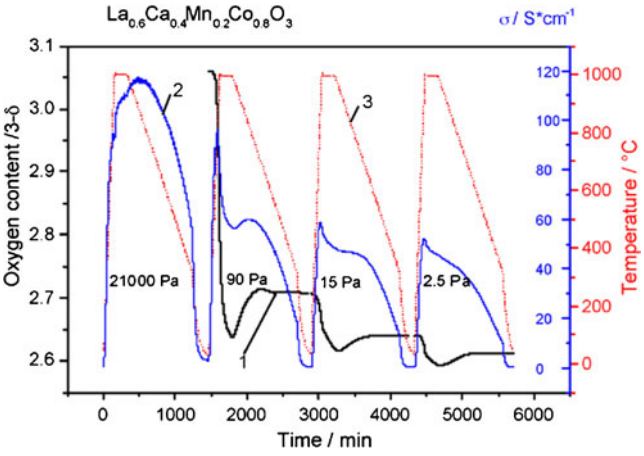

Fig. 32 Oxygen content (*1*), electrical conductivity (*2*), and temperature (*3*) of the ceramic sample during treatment in gas flows at different oxygen partial pressures [92]

$La_{0.4}Sr_{0.6}FeO_{3-\delta}$ determined by different methods including OSEC in the temperature range 700–900 °C at oxygen concentration varying from 1×10^{-4} to 2×10^{-3} bar [69].

The oxygen nonstoichiometry and electrical conductivity of the series of lanthanum–strontium nickelates [69–72] have been investigated using OXYLYT™ devices. Some of the results obtained in the $La_{2-x}Sr_xNiO_{4\pm\delta}$ system are presented in Fig. 24. The pO_2 dependence of oxygen nonstoichiometry and electrical conductivity for $La_2NiO_{4\pm\delta}$ are given in Fig. 25. A very stable composition in the $La_{2-x}Sr_xNiO_{4\pm\delta}$ system at x=0.4 was discovered. The nickelates studied are p-type conductors whose conductivity decreases with temperature, as in metals. The oxygen permeability of nickelates with x=0–0.4 measured with a pO_2 gradient between 0.21×10^5 and 200 Pa increases in accordance with increasing range of oxygen nonstoichiometry. The highest permeation of about 8×10^{-7} mol $cm^{-2}s^{-1}$ at 1,000 °C was found for $La_2NiO_{4\pm\delta}$.

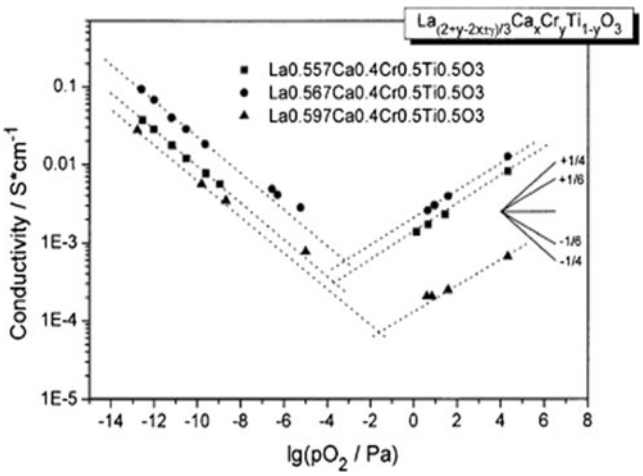

Fig. 31 Electrical conductivity some $La_{0.567\pm\gamma}Ca_4Cr_{0.5}Ti_{0.5}O_3$ ceramic samples at 900 °C [88]

Oxygen nonstoichiometry and electrical conductivity of the $Pr_{2-x}Sr_xNiO_{4\pm\delta}$ series with x=0–1.0 have been investigated in Ar/O_2 (pO_2=2.5 to 21,000 Pa) in the temperature range 20–1,000 °C [73–75]. The equilibrium values of oxygen nonstoichiometry and electrical conductivity of these nickelates were determined as functions of temperature and oxygen partial pressure. In the investigated temperature and pO_2 ranges, the nickelates appear to be p-type semiconductors (Fig. 26). The conductivity of the $Pr_{2-x}Sr_xNiO_{4\pm\delta}$ samples correlates to the middle oxidation state of nickel cations. The samples with x=0.9 show the highest conductivities of 170–700 S/cm at 500–900 °C and pO_2= 2.5–21,000 Pa. In these samples, the middle oxidation state of nickel is closest to 3.0+. The nickelates with x=0.3–0.5 show insignificant pO_2 conductivity dependencies. The $Pr_{1.8}Sr_{0.2}NiO_{4\pm\delta}$ and $Pr_{1.7}Sr_{0.3}NiO_{4\pm\delta}$ nickelates show anomalies in conductivity versus oxygen partial pressure,

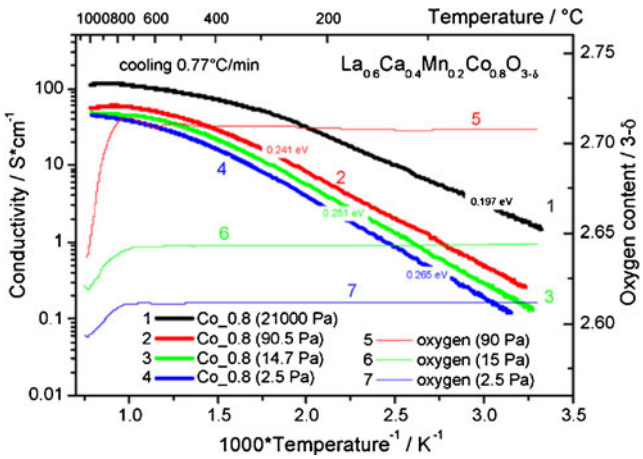

Fig. 33 Conductivity (*1–4*) and oxygen content (*5–7*) of the ceramic sample during cooling in gas flows at different oxygen partial pressures [92]

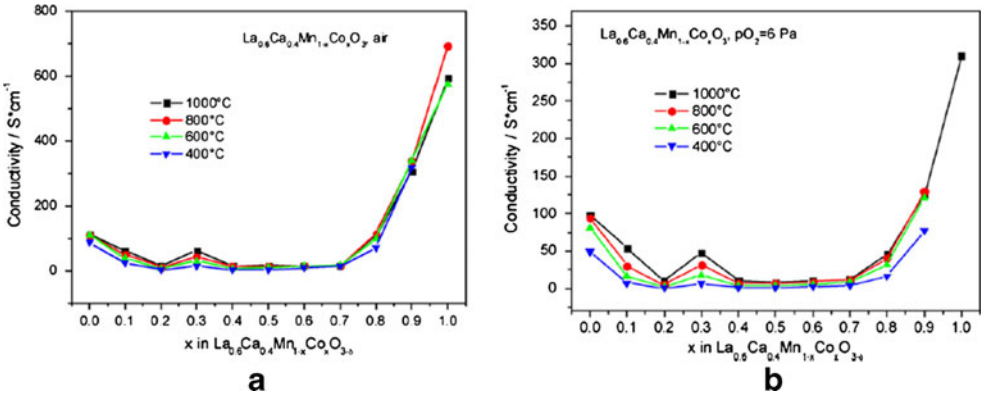

Fig. 34 Co-content dependence of conductivity for the $La_{0.6}Ca_{0.4}Mn_{1-x}Co_xO_{3-\delta}$ samples measured in air (**a**) and in Ar/O_2 flow at pO_2=6 Pa (**b**) at different temperatures [92]

which can be related to transformations between orthorhombic and tetragonal crystal structure.

A series of $La_{2-x}Sr_xCoO_{4\pm\delta}$ (x=0.5–1.5) compounds as powders and ceramic shapes showed reversible oxygen desorption–sorption behavior in argon during heating and cooling between 300 and 1,050 °C [76]. The amount of exchanged oxygen δ was found to be a function of Sr content, x. In the range $0.5<x<0.8$, the amount of exchanged oxygen decreased to 0, and from $0.9<x<1.5$, it increased to a maximum value. At 850 °C, the $LaSrCoO_{4\pm\delta}$ compound (x=1) showed a maximum conductivity of 160 Scm^{-1}.

Hagenhammer et al. have investigated the reoxidation process of donor-doped [77–79] and acceptor-doped [79] $BaTiO_3$ ceramics at temperatures of up to 1,500 °C in flowing gas at pO_2=2.4–260 Pa. During an investigation of the sintering process of $Ba_{1-x}La_xTiO_3$ ceramics ($0<x<0.05$), three different oxygen release phenomena were observed: the first due to the formation of Schottky-type oxygen vacancies, the second caused by the incorporation of the donor impurity during grain growth, and finally, an irreversible release with an onset temperature between 1,000 and 1,150 °C. The reason for this was not clear (Fig. 27) [78, 79].

Oxygen stoichiometry, total electrical conductivity, and oxygen diffusion mobility were measured for certain compositions for the cation stoichiometric $Ca_{1-x}La_xCr_{1-y}Ti_yO_{3-\delta}$ and A-site-deficient $La_{(2+y-2x)/3}Ca_xCr_yTi_{1-y}O_{3-\delta}$ systems at temperatures of 20–1,000 °C and at oxygen pressures of 1×10^{-14} to 0.21×10^5 Pa [80–88]; Figs. 28, 29, 30, and 31 illustrate something of this SEC.

The A-site-deficient samples show a higher sintering ability in comparison with the cation stoichiometric compositions, and in contrast to the latter, they can be prepared in a dense state in air at temperatures of 1,200–1,300 °C. The oxygen mobility of these can be characterized by chemical diffusion coefficients equal to $(1–9)\times10^{-9}$ cm^2s^{-1} at 900 °C and pO_2=1,000–21,000 Pa. It seems that the low oxygen mobility of the A-site-deficient chromites–titanates turns out to be the only disadvantage of these compositions with respect to their application as anode material for solid oxide fuel cells (SOFCs) [88].

It has been found that the high electrical conductivity of $La_{1-x}Ca_xTiO_{3-\delta}$ under reducing conditions and the high catalytic activity of $La_{0.1}Ca_{0.9}Ti_{1-x}Ru_xO_{3-\delta}$ for the oxidation of hydrocarbons might possibly be combined to form an efficient multilayer SOFC anode [89].

The high thermal and chemical stability of the compounds in the $La_{1-x}Ca_xCr_{1-y}Ti_yO_3$ system at high temperature in a broad oxygen partial pressure range, coupled with their sufficiently high electrical conductivity under reducing conditions, give some hope for increasing their catalytic activity by doping with small amounts of other catalytic active cations on B-sites and for possibilities of using these compounds as SOFC anode materials.

Double B perovskite compounds in the system $La_{0.6}Ca_{0.4}Mn_{1-x}Me_xO_{3-\delta}$ with Me=Fe, Co, Ni and x=0–0.6 were

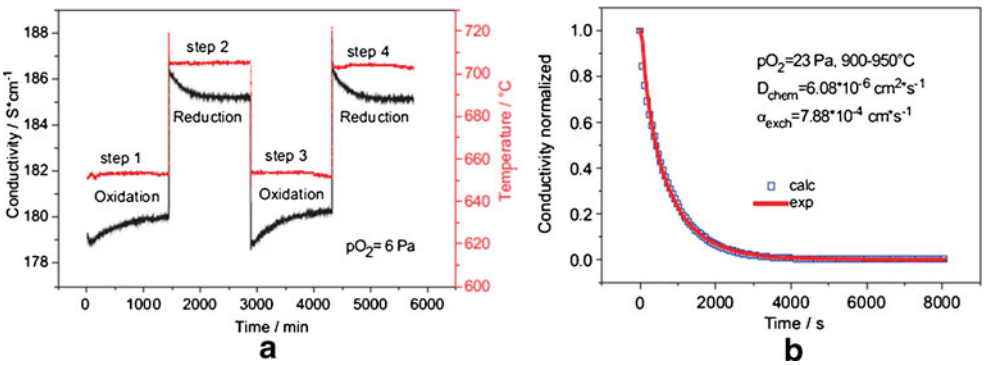

Fig. 35 A typical measurement of conductivity relaxation during stepwise change in temperature (**a**) and fitting result for experimental and theoretical data (**b**) [94]

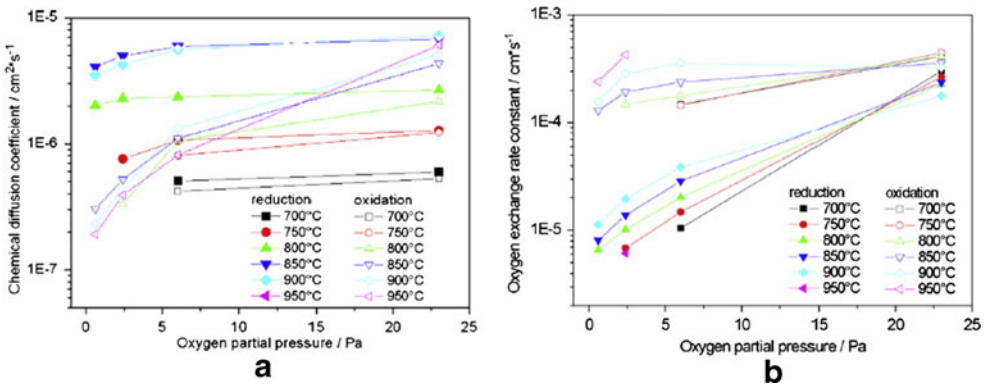

Fig. 36 Oxygen partial pressures dependence of chemical diffusion coefficients (**a**) and oxygen exchange rate constants (**b**) measured at different temperatures [94]

synthesized and their conductivity, oxygen stoichiometry, and defect structure were investigated as a function of temperature and oxygen concentration in the gas phase [89–91]. Some results are presented in Figs. 32, 33, and 34 for Me=Co. Replacement of Mn by Me cations is accompanied by a considerable decrease of electrical conductivity. Lower conductivities of Me-containing compositions compared with those of $La_{0.6}Ca_{0.4}MnO_{3-\delta}$ are explained by stronger polarization of the $–Mn^{(\alpha+\gamma)+}–O^{\alpha-}–Me^{(\alpha-\gamma)+}–O^{\alpha-}–$ fragments of the $–O^{\alpha-}–Mn^{\alpha+}–O^{\alpha-}–Mn^{\alpha+}–O^{\alpha-}–Mn^{(\alpha+\gamma)+}O^{\alpha-}–Me^{(\alpha-\gamma)+}–O^{\alpha-}–$ chains in comparison with the $–O^{\alpha-}–Mn^{\alpha+}–O^{\alpha-}–Mn^{\alpha+}–O^{\alpha-}–$ chains without Me cations because of different electronegativities of Me and Mn. The type and magnitude of the electrical conductivity of the $La_{0.6}Ca_{0.4}Mn_{1-x}Me_xO_{3-\delta}$ series were found to be functions of the $[Mn^{4+}]/[Mn^{3+}]$ and $[Me^{3+}]/[Me^{2+}]$ ratios. Mn^{4+} and Me^{2+} cations are possible point defects which determine the p-type and n-type conductivity of the compounds, respectively.

Thermal stability, thermal expansion, oxygen nonstoichiometry, electrical conductivity, and diffusion characteristics of $LaNi_{0.4}Fe_{0.6}O_{3-\delta}$ [92] and $PrNi_{0.6}Fe_{0.4}O_{3-\delta}$ [93] ceramic samples have been investigated as functions of temperature (20–1,000 °C) and oxygen partial pressure (0.5–21,000 Pa). The measurements show that the compositions were phase stable at $pO_2>1$ Pa up to 1,000 °C and show p-type semiconductivity with a low conductivity versus pO_2 dependence. The perovskites have been found to have comparable thermal expansion coefficients to those of commonly used solid electrolytes such as CeO_2- and ZrO_2-based oxides. In the chemical diffusion experiments with $PrNi_{0.6}Fe_{0.4}O_{3-\delta}$ ceramics, a higher oxygen diffusion mobility was observed during reduction processes compared with those during oxidation. This was explained by the previously known formation of neutral defect clusters. Some results of relaxation experiments on gas-dense $PrNi_{0.6}Fe_{0.4}O_{3-\delta}$ ceramics samples are shown in Figs. 35 and 36.

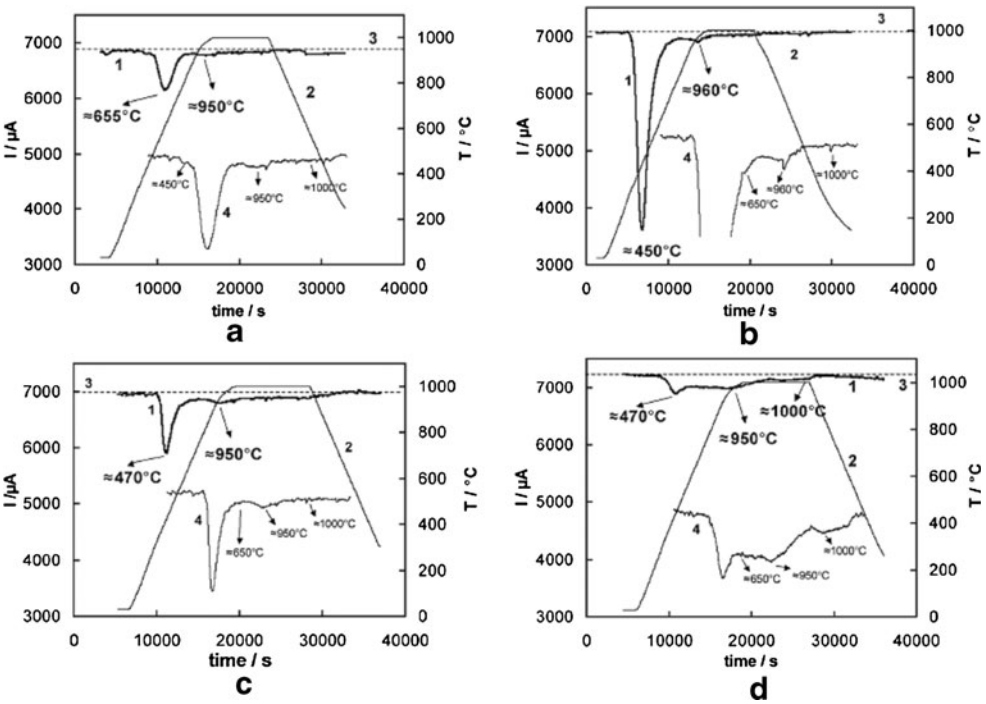

Fig. 37 Coulometric titration of $CaTi_{1-x}Fe_xO_{3-\delta}$: **a** x=0.05, **b** x=0.20, **c** x=0.40, and **d** x=0.60. *1* coulometric current, *2* temperature, *3* coulometric current base line, *4* insets for qualitative indication of peak location [95]

Ordered and disordered phases of the system $Ca(Ti,Fe)O_{3-\delta}$ were prepared and characterized by XRD, Mössbauer spectroscopy, oxygen coulometric titration, and oxygen permeation measurements [94]. The number of oxygen vacancies per formula unit obtained from the Mössbauer spectra, assuming fully ionized oxygen vacancies, was confirmed by oxygen stoichiometry changes determined using an OXYLYT™ device. The combination of Mössbauer spectroscopy and coulometric titration was found to provide useful information on the defect chemistry of iron- (or tin)-containing materials. Figure 37 illustrates some coulometric experiments. Some other perovskite-type mixed oxides investigated by means of SEC are described elsewhere [95–97].

Investigations of the oxygen stoichiometry and conductivity of Nb_2O_5 and In_2O_3 have been carried out using an OXYLYT™ device [98]. The results show that the oxygen stoichiometry of Nb_2O_5 remains nearly constant even at very low oxygen partial pressures ($pO_2 < 10^{-7}$ Pa). The oxygen loss from In_2O_3 was much higher at low oxygen partial pressures where no equilibrium was found. This oxide is not stable at low pO_2. Another significant property of Nb_2O_5 is the fast response of conductivity to changing oxygen partial pressures.

Oxygen permeation measurements were carried out using an OXYLYT™ device on a $Gd_{0.85}Ca_{0.15}AlO_{3-\delta}$ specimen in the temperature range 400–900 °C as a function of oxygen partial pressure from 18 to 10^5 Pa [99]. The investigations suggest that $Gd_{0.85}Ca_{0.15}AlO_{3-\delta}$ is predominantly an oxygen ion conductor with an ionic conductivity slightly below that of YSZ.

Novitskaya et al. [100] have investigated the new black quaternary oxide $Sr_5BiNi_2O_{9.6}$. Thermogravimetry and high-temperature oxygen coulometry showed that this compound has variable oxygen content as a function of temperature and oxygen pressure and ultimately decomposes when heated at low oxygen pressure above 800 °C.

Conclusions

As an alternative to thermogravimetry, chemical analysis, spectroscopy, and X-ray or neutron diffractometry, OSEC is universally useful for the quantitative investigation of different oxygen exchange processes for scientific measurements in the chemical and biochemical industries, in metallurgy, in the production of semiconductors and special ceramics, and for other processes. It can be used for the creation of gas atmospheres and gas flows with well-determined oxygen partial pressure from 10^{-20} to 10^6 Pa, for the determination of oxygen permeability through ceramic, metallic, or polymer membranes, and for the measurement of small amounts of humidity and of hydrogen, hydrocarbons, or other gases in mixed gaseous media.

References

1. DeFord DD, Bowers RC (1958) Anal Chem 30:613
2. DeFord DD (1960) Anal Chem 32:531R
3. Scholz F (ed) (2010) Electroanalytical methods (2nd edn). Springer, Berlin, p 147
4. Tretyakov YD, Rapp R (1969) Trans Met Soc AIME 245:1235
5. Ahn BT, Gür TM, Huggins RA, Beyers R, Engler EM, Grant PM, Parkin SSP, Lim G, Ramirez ML, Roche KP, Vasquez JE, Lee VY, Jakowitz RD (1988) Phisica C 153–155:590
6. Li J, Gür TM, Sinclair R, Rosenblum SS, Hayashi H (1994) Solid State Ion 73:185
7. Patrakeev MV, Leonidov IA, Kozevnikov LV (1995) Solid State Ion 82:5
8. Hartung R (1973) Z Phys Chem 254:393
9. Lankhorst MHR, Bouwmeester HJM, Verweij H (1997) Solid State Ion 96:21
10. Lankhorst MHR, Bouwmeester HJM (1997) J Electrochem Soc 144:1261
11. Lade K, Jacobsen T (1994) Solid State Ion 72:218
12. Patrakeev MV, Mitberg EB, Lakhtin AA, Leonidov IA (1998) Ionics 4:191
13. Patrakeev MV, Leonidov IA, Lakhtin AA, Kozhevnikov VL (1995) J Solid State Chem 120:146
14. Fouletier J, Vitter G, Kleitz M (1975) J Appl Electrochem 5/2:111
15. Ruka RJ, Weissbart J (1968) US Patent 3,400,054, 3 Sept
16. Antonsen O, Baukal W, Fischer W (1966) Brown Boveri Rev 53:21
17. Bulliere C (1966) Etude du pompage ectrochimique de l'oxygene dans une cellule a oxyde electrolyte solide. Diplome d'Etudes Superieures, Grenoble
18. Besson J, Deportes C, Kleitz M (1969) France Patent 1,580,819
19. Beekmans NM, Heyne L (1971) Philips Tech Rev 31:51
20. Rapp RA (1972) US Patent 3,699,032, 17 Oct
21. Hartung R, Möbius HH (1967) Z Chem 7:473
22. Besson J, Bonnat M, Deportes C, Kleitz M (1972) Fr Addn 2:110
23. Fouletier J, Seinera H, Kleitz M (1974) J Appl Electrochem 4:305
24. Fouletier J, Seinera H, Kleitz M (1975) J Appl Electrochem 5:177
25. Teske K, Gläser W (1975) Mikroch Acta [Wien] I:653
26. Bode M, Teske K, Ullmann H (1994) GIT Fachzeitschrift Labor 38:495
27. Teske K, Ullmann H, Rettig D (1983) J nucl mat 116:260
28. Teske K, Nebelung C (1985) Thermoch acta 96:453
29. Teske K, Nebelung C, Kapshukov II, Sudakov LV, Bevz AS (1989) J nucl mat 168:97
30. Teske K, Popp P, Baumbach J (1986) J Chromatography 360:417
31. Teske K, Nebelung C, Ullmann H, Kapshukov II, Sudakov LV, Bevz AS (1992) J nucl mat 188:26
32. Ducroux R, Baptiste P (1981) J nucl mat 97:333
33. Kapshukov II, Lyalishkin NV, Sudakov LV, Bevz AS, Skiba OV (1990) J Radioanal Nucl Chem Articles 143:213
34. Lang HJ, Künstler K, Tomandl G (1999) Solid State Ion 119:127
35. Teske K, Oppermann H, Stoever G (1984) Z Anorg Allg Chem 51:72
36. Bode M, Haptmann P, Teske K, Weigel FD (1991) Sens Actuat B 4:407
37. Kaufmann H, Fickert J, Natsik VD, Pal-Val PP, Matz W, Rudolph K, Teske K (1991) Phys Stat Sol (a) 123:K111
38. Teske K, Anwand W, Fischer K (1993) J All Comp 195:671
39. Günther W, Schöllhorn R (1996) Physica C: Supercond 271:241
40. Günther W (1997) Schöllhorn R Solid State Ionics 101–103:1335
41. Kalanda NA, Trukhan VM, Marenkin SF (2002) Inorg Mat 38:694
42. Zhigunov DI, Shiryaev SV, Kurnevich LA, Kalanda NA, Kurochkin LA, Barilo SN, Vashuk VV, Smakhtin LA (1999) J Cryst Growth 198–199:605

43. Pankov V, Kalanda N, Truchan V, Zhigunov D, Babushkin O (2002) Physica C: Supercond 377:521
44. Steinbrück M, Feltz A (1992) J Mat Sci Let 11:216
45. Vashook VV, Zinkevich MV, Ullmann H, Paulsen J, Trofimenko N, Teske K (1997) Solid State Ion 99:23
46. Teske K, Ullmann H, Trofimenko N (1997) J Therm Anal 49:1211
47. Trofimenko NE, Ullmann H, Paulsen J, Müller R (1997) Solid State Ion 99:201
48. Trofimenko NE, Paulsen J, Ullmann H, Müller R (1997) Solid State Ion 100:183
49. Trofimenko NE, Ullmann H (2000) J Europ Ceram Soc 20:1241
50. Rossberg, Oppermann H, Glathe F (1987) Z anorg Allgem Chem 554:166
51. Bonsdorf G, Schäfer K, Teske K, Langbein H, Ullmann H (1998) Solid State Ion 110:73
52. Paulsen JM (1999) Dahn JR Chem Mat 11:3065
53. Künstler K, Lang HJ, Maiwald A, Tomandl G (1998) Solid State Ion 107:221
54. Ziesche S, Jurk R, Trofimenko N, Kusnezoff M (2008) Solid State Ion 179:1351
55. Trofimenko N, Ullmann H (1999) Solid State Ion 118:215
56. Trofimenko N, Ullmann H (1999) Solid State Ion 124:263
57. Khorkounov B (2004) Thesis
58. Vasylechko L, Vashook V, Savytskii D, Senyshyn A, Niewa R, Knapp M, Ullmann H, Berkowski M, Matkovskii A, Bismayer U (2003) J Sol State Chem 172:396
59. Hartley A, Sahibzada M, Weston M, Metcalfe IS, Mantzavinos D (2000) Catal Today 55:197
60. Sahibzada M, Morton W, Hartley A, Mantzavinos D, Metcalfe IS (2000) Solid State Ion 136–137:991
61. Hartley A, Sahibzada M, Metcalfe IS (2000) Solid State Ion 136–137:127
62. Mantzavinos D, Metcalfe IS, Sahibzada M (2000) Solid State Ion 134:103
63. Sahibzada M, Mantzavinos D, Hartley A, Morton W, Metcalfe IS (2000) Trans IChemE, Part A 78:965
64. Scott SP, Mantzavinos D, Hartley A, Sahibzada M, Metcalfe IS (2002) Solid State Ion 152–153:777
65. Sitte W, Bucher E, Benisek A, Preis W (2001) Spectroch Acta Part A 57:2071
66. Bucher E, Jantscher W, Benisek A, Sitte W, Preis W, Rom I, Hofer F (2001) Solid State Ion 141–142:375
67. Preis W, Bucher E, Sitte W (2002) J Pow Sour 106:116
68. Preis W, Bucher E, Sitte W (2004) Solid State Ion 175:393
69. Vashook VV, Yushkevich II, Kokhanovsky LV, Makhnach LV, Tolochko SP, Kononyuk IF, Ullmann H, Altenburg H (1999) Solid State Ion 119:23
70. Vashook VV, Trofimenko NE, Ullmann H, Makhnach LV (2000) Solid State Ion 131:329
71. Makhnach LV, Pankov VV, Strobel P (2008) Mater Chem Phys 111:125
72. Vashook VV, Tolochko SP, Yushkevich II, Makhnach LV, Kononyuk IF, Altenburg H, Hauck J, Ullmann H (1998) Solid State Ion 110:245
73. Vashook V, Zosel J, Wen TL, Guth U (2006) Solid State Ion 177:1827
74. Vashook V, Girdauskaite E, Zosel J, Wen TL, Ullmann H, Guth U (2006) Solid State Ion 177:1163
75. Vashook V, Vasylechko L, Girdauskaite E, Zosel J, Wen TL, Ullmann H, Guth U (2006) Mat Sci Tech: Mater Syst 1:212
76. Vashook VV, Ullmann H, Olshevskaya OP, Kulik VP, Lukashevich VE, Kokhanovskij LV (2000) Solid State Ion 138:99
77. Langhammer HT, Song QM, Abicht HP (2001) J Eur Ceram Soc 21:1893
78. Langhammer H, Song QM, Felgner KH, Abicht HP (2002) Solid State Sci 4:197
79. Langhammer HT, Makovec D, Pu Y, Abicht HP, Drofenik M (2006) J Eur Ceram Soc 26:2899
80. Vashook V, Vasylechko L, Knapp M (2003) J All Comp 354:13
81. Vashook V, Vasylechko L, Ullmann H, Guth U (2002) J All Comp 340:263
82. Vashook V, Vasylechko L, Ullmann H, Guth U (2003) Solid State Ion 158:317
83. Vashook V, Vasylechko L, Zosel J, Guth U (2003) Solid State Ionics 159:279
84. Vashook V, Zosel J, Preis W, Sitte W, Guth U (2004) Solid State Ion 175:441
85. Vashook V, Vasylechko L, Zosel J, Müller R, Ahlborn E, Guth U (2004) Solid State Ion 175:151
86. Vashook V, Vasylechko L, Zosel J, Gruner W, Ullmann H, Guth U (2004) J Solid State Chem 177:3784
87. Vashook V, Vasylechko L, Trofimenko N, Kuznecov M, Otchik P, Zosel J, Guth U (2006) J All Comp 419:271
88. Vashook V, Zosel J, Müller R, Shuk P, Vasylechko L, Ullmann H, Guth U (2006) Fuel Cells 06:293
89. Vashook V, Franke D, Vasylechko L, Zosel J, Rebello J, Ahlborn K, Fichtner W, Schmidt M, Wen TL, Guth U (2008) Solid State Ion 179:1101
90. Vashook V, Franke D, Zosel J, Ahlborn K, Vasylechko L, Fichtner W, Guth U (2008) Solid State Ion 179:135
91. Vashook V, Franke D, Zosel J, Vasylechko L, Schmidt M, Guth U (2009) J All Comp 487:577
92. Chen JY, Rebello J, Vashook V, Trots D, Wang SR, Wen TL, Zosel J, Guth U (2011) Solid State Ion 192:424
93. Rebello J, Vashook V, Trots D, Guth U (2011) J Pow Sour 196:3705
94. Figueiredo FM, Waerenborgh J, Kharton VV, Näfe H, Frade JR (2003) Solid State Ion 156:371
95. Ullmann H, Trofimenko N (1999) Solid State Ion 119:1
96. Ullmann H, Trofimenko N, Naoumidis A, Stöver D (1999) J Eur Ceram Soc 19:791
97. Al Daroukh M, Vashook VV, Ullmann H, Tietz F, Arual Raj I (2003) Solid State Ion 158:141
98. Zosel J, Ahlborn K, Müller R, Westphal D, Vashook V, Guth U (2004) Solid State Ion 169:115
99. Sinha A, Näfe H, Sharma BP, Gopalan P (2008) J Electrochem Soc 155:B309
100. Novitskaya M, Makhnach L, Ivashkevich L, Pankov V, Klein H, Rageau A, David J, Gemmi M, Hadermann J, Strobel P (2011) J Solid State Chem 184:3262
101. Lankhorst MHR, ten Elshof JE (1997) J Solid State Chem 130:302